AD-A194 662

NAVAL POSTGRADUATE SCHOOL
Monterey, California

②

DTIC FILE COPY

SDTIC **D**
ELECTE
JUN 2 3 1988
C&D

THESIS

CHARACTERIZATION OF HIGH DAMPING Fe-Cr-Mo
AND Fe-Cr-Al ALLOYS FOR NAVAL
SHIPS APPLICATION

by

David Bruce Ferguson

March 1988

Thesis Advisor: J. Perkins

A194662

REPORT DOCUMENTATION PAGE

1a REPORT SECURITY CLASSIFICATION UNCLASSIFIED		1b RESTRICTIVE MARKINGS		
2a SECURITY CLASSIFICATION AUTHORITY		3 DISTRIBUTION/AVAILABILITY OF REPORT Approved for public release; distribution is unlimited		
2b DECLASSIFICATION/DOWNGRADING SCHEDULE				
4 PERFORMING ORGANIZATION REPORT NUMBER(S)		5 MONITORING ORGANIZATION REPORT NUMBER(S)		
6a NAME OF PERFORMING ORGANIZATION Naval Postgraduate School	6b OFFICE SYMBOL (If applicable) Code 69	7a NAME OF MONITORING ORGANIZATION Naval Postgraduate School		
6c ADDRESS (City, State, and ZIP Code) Monterey, California 93943-5000		7b ADDRESS (City, State, and ZIP Code) Monterey, California 93943-5000		
8a NAME OF FUNDING/SPONSORING ORGANIZATION	8b OFFICE SYMBOL (If applicable)	9 PROCUREMENT INSTRUMENT IDENTIFICATION NUMBER		
8c ADDRESS (City, State, and ZIP Code)		10 SOURCE OF FUNDING NUMBERS		
		PROGRAM ELEMENT NO	PROJECT NO	TASK NO	WORK UNIT ACCESSION NO

11 TITLE (Include Security Classification)

CHARACTERIZATION OF HIGH DAMPING Fe-Cr-Mo AND Fe-Cr-Al ALLOYS FOR NAVAL SHIPS APPLICATION

12 PERSONAL AUTHOR(S)

Ferguson, David B.

13a TYPE OF REPORT Master's Thesis	13b TIME COVERED FROM _____ TO _____	14 DATE OF REPORT (Year, Month, Day) 1988, March	15 PAGE COUNT 100

16 SUPPLEMENTARY NOTATION

The views expressed in this thesis are those of the author and do not reflect the official policy or position of the Department of Defense or the U.S. Government.

17	COSATI CODES		18 SUBJECT TERMS (Continue on reverse if necessary and identify by block number)
FIELD	GROUP	SUB-GROUP	Damping; Ship Silencing; Ferritic Stainless Steels; Ti-Ni

19 ABSTRACT (Continue on reverse if necessary and identify by block number)

The metallurgical basis for high damping in Fe-Cr-based alloys was investigated. Two alloys similar to VACROSIL-010 were studied, with compositions of 84.7 Fe-11.44 Cr-2.91 Al and 84.8 Fe-11.65 Cr-2.92 Mo. The strain dependence of specific damping capacity (SDC) was evaluated using a modified version of the resonant dwell technique. Heat treatment variations were introduced by annealing in argon gas at temperatures between 950°C and 1100°C and then furnace cooling. Cantilever beam specimens were evaluated for SDC at their first three resonant modes (0-1,000 Hz) at room temperature. Changes in damping capacity were correlated with the results of tensile hysteresis testing and dilatometry.

20 DISTRIBUTION/AVAILABILITY OF ABSTRACT ☒ UNCLASSIFIED/UNLIMITED ☐ SAME AS RPT ☐ DTIC USERS	21 ABSTRACT SECURITY CLASSIFICATION Unclassified	
22a NAME OF RESPONSIBLE INDIVIDUAL Prof. Jeff Perkins	22b TELEPHONE (Include Area Code) (408) 646-2216	22c OFFICE SYMBOL Code 69Ps

i

Characterization of High Damping Fe-Cr-Mo and
Fe-Cr-Al Alloys for Naval Ships Application

by

David Bruce Ferguson
Lieutenant Commander, United States Navy
B.S., Mathematics/Systems, Vanderbilt University, 1977

Submitted in partial fulfillment of the
requirements for the degree of

MASTER OF SCIENCE IN MECHANICAL ENGINEERING

from the

NAVAL POSTGRADUATE SCHOOL
March 1988

Author: _____
David B. Ferguson

Approved by: _____
J. Perkins, Thesis Advisor

_____
Anthony J. Healey, Chairman
Department of Mechanical Engineering

_____
Gordon E. Schacher
Dean of Science and Engineering

ii

ABSTRACT

The metallurgical basis for high damping in Fe-Cr-based alloys was investigated. Two alloys similar to VACROSIL-010 were studied, with compositions of 84.7 Fe-11.44 Cr-2.91 Al and 84.8 Fe-11.65 Cr-2.92 Mo. The strain dependence of specific damping capacity (SDC) was evaluated using a modified version of the resonant dwell technique. Heat treatment variations were introduced by annealing in argon gas at temperatures between 950°C and 1100°C and then furnace cooling. Cantilever beam specimens were evaluated for SDC at their first three resonant modes (0-1,000 Hz) at room temperature. Changes in damping capacity were correlated with the results of tensile hysteresis testing and dilatometry.

Accesion For		
NTIS CRA&I	☑	
DTIC TAB	☐	
Unannounced	☐	
Justification		
By		
Distribution /		
Availability Codes		
Dist	Avail and / or Special	
A-1		

DTIC COPY INSPECTED 6

iii

TABLE OF CONTENTS

LIST OF TABLES

LIST OF FIGURES

ACKNOWLEDGMENTS

I. INTRODUCTION

A. GENERAL

The U.S. Navy is currently investigating the reduction
of noise and vibration in both submarine and surface ship
design. For both platforms it is desirable to remain
quieter than ambient noise to minimize detection. It is
also important to minimize noise interference with one's own
sensors. Noise reduction may also improve component fatigue
life and reduce hazards to personnel due to high ambient
noise levels.

Schetky and Perkins [Ref. 1] list three primary methods
of reducing noise and vibration:

1. Isolation of the sources (moving parts) and the
   surrounding surfaces that can radiate energy.

2. Dissipation of the energy transmitted through the
   structure, using isolation pads.

3. Construction of structural or machine components
   themselves from energy absorbing structural materials.
   These high damping materials would serve the dual
   purposes of structural support and noise abatement.

The problems inherent in the first two methods are that
resilient mounts, hangers, and encapsulating shrouds take up
space, add weight, and increase the complexity of
maintaining the system. Method three can eliminate these
problems, but design with high damping materials is an
uncertain and potentially difficult matter at present. For
one thing, the mechanisms of damping are not well

1

understood, and the influence of important factors such as temperature, strain, heat treatment, and deformation are incompletely characterized.

The U.S. Navy is currently quite interested in investigating the damping properties of commercial high damping alloys, including correlations between the relevant microstructural and physical properties.

B. OBJECTIVES

High damping alloys have been investigated for over 40 years, yet information on the damping properties of Fe-Cr and other ferromagnetic high damping alloys is relatively limited [Ref. 2]. A new alloy has been introduced commercially by Vacuumschmelze, G.M.B.H. (VAC), of Hanau, West Germany. This alloy has the registered trade name of VACROSIL-010, with two diverse compositions, Fe-Cr-Al and Fe-Cr-Mo (this latter a corrosion-resistant grade) [Ref. 3]. The alloys used in this study were not VACROSIL per se (i.e., were not supplied by Vacuumschmelze, G.M.B.H.), but rather were "clones" of the two alloy versions. These two versions of the alloy will be referred to in this report as "Fe-Cr-Al" and "Fe-Cr-Mo." The corrosion resistant version is of particular interest for marine applications.

The purpose of this research is to continue to explore the damping characteristics of these alloys from a metallurgical point of view. The following objectives guided this research:

1. To assemble a damping test apparatus and develop standard, reproducible test procedures.

2. To determine the effect of heat treatment on the relationship between applied strain and damping capacity under random vibration conditions.

3. To analyze and compare the physical properties of the Fe-Cr-Al and Fe-Cr-Mo alloys.

4. To attempt to correlate the damping capacity with phase changes using a dilatometer.

5. To investigate possible pseudoelastic effects at low levels during tensile loading.

C. BACKGROUND

All materials exhibit an ability to dampen the propagation of energy. However, in most metals the damping capacity is quite low, on the order of 1% to 10%. Recently, alloys have been developed with damping capacities well in excess of 10%. These high damping ("quiet metal") alloys show good potential for use in noise and vibration control applications.

These alloys include Mn-Cu-based alloys; ferromagnetic alloys from the Fe-Cr, Fe-Co, and Co-Ni system; and shape memory alloys from the Ti-Ni, Cu-Zn-Al, and Cu-Al-Ni systems. Research on these systems has led to the introduction of various commercial alloys for high damping applications. From the Mn-Cu system has come the alloys called "INCRAMUTE" (International Copper Research Association) and "SONOSTON" (British Stone Marine Manganese Ltd.). SONOSTON has been used for ships propellers in

3

Europe while INCRAMUTE has been used for noise reduction in tools and machinery.

Several ferromagnetic alloys have been introduced commercially, including "SILENTALLOY" (Toshiba Co.), "TRANQUALLOY" (Nippon Steel Co.), "VACROSIL" (Vacuumschmelzer G.M.B.H.), and "NIVCO" (Westinghouse). These alloys show promise for vibration control in automobiles and electrical machinery.

Recent research at the Naval Postgraduate School has included work on SONOSTON [Refs. 4,5], INCRAMUTE [Refs. 2,5], and a VACROSIL-type alloy [Ref. 6]. This study continues the investigation of VACROSIL-type alloys.

The damping mechanism for the Fe-Cr-based alloys has been shown to be based primarily on the ferromagnetic properties of the alloy [Refs 3,7-14]. In particular, de Batiste [Ref. 8] states that the damping is related to the interaction of the applied stress field and the domain boundaries. He also relates the effects of varying parameters such as temperature, amplitude, frequency and field strength on damping capacity.

The present research investigates the effects of heat treatment and strain on damping of two Fe-Cr-based alloys.

D. DAMPING MECHANISMS

   1. <u>Macrostructural Damping</u>

      a. Parameters

      The dissipation of energy by a material is known
as damping. The energy loss per cycle divided by the peak
potential energy is defined as the specific damping capacity
(SDC) [Ref. 15:p. 70]. Several parameters are used to
describe vibration damping.

      (1) <u>General Equation</u>. For a simple model of a
linear system with one degree of freedom and viscous
damping, the general differential equation is of the form
[Ref. 15:p. 25]:

$$m\ddot{x} + c\dot{x} + kx = F \qquad (1.1)$$

where:

      m = mass

      c = viscous damping coefficient

      k = spring constant

      F = excitation

      x = displacement

$\dot{x}$ and $\ddot{x}$ = the first and second derivatives of
                displacement with respect to time.

      (2) <u>Natural Frequency (ω_n)</u>.

$$\omega_n = (k/m)^{1/2} \qquad (1.2)$$

5

The mode 1 resonant frequency is called the natural frequency. The characteristic response for the first three modes is shown in Figure 1.1.

(3)   <u>Critical Damping Factor (C_c)</u> [Ref. 15:p. 27].

$$C_c = 2m\omega_n \qquad (1.3)$$

(4)   <u>Damping Ratio of (ζ)</u> [Ref. 15:p. 27].

$$\zeta = c/C_c \qquad (1.4)$$

If the excitation (F) is represented in the complex form ($F^{i\omega t}$) and $c = 2m\omega_n\zeta$, then the steady state solution to Equation 1.1 is of the form [Ref. 16:p. 130]:

$$x = Xe^{i(\omega t-\phi)} = F^{i\omega t}/[(k-m\omega^2) + i\omega c] \qquad (1.5)$$

(5)   <u>Logarithmic Decrement (δ)</u>.

$$\delta = \ln(a_i/a_{i+1}) \qquad (1.6)$$

The logarithmic decrement is defined as the natural logarithm of the ratio of any two successive amplitudes of vibration. Greater accuracy can be obtained if the ratio of two amplitudes n cycles apart is used [Ref. 17:p. 68]. The logarithmic decrement is now expressed as:

6

MODE 1

MODE 2

MODE 3
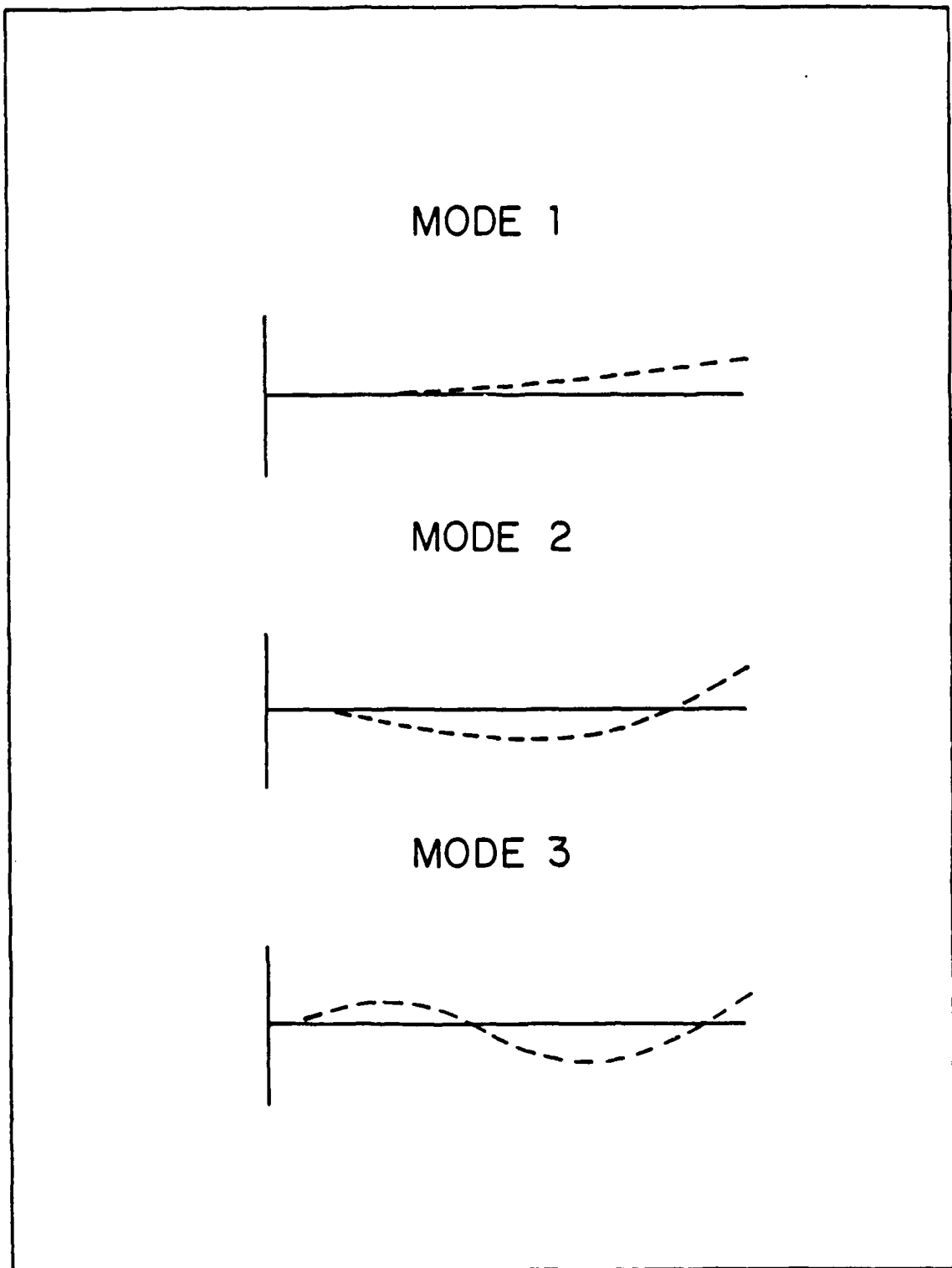
Figure 1.1   Characteristic Response of Cantilever Beam
to First Three Modes of Excitation

7

$$\delta = 1/n \ln(a_i/a_{i+n}) \qquad (1.7)$$

(6) Normalized Bandwidth.

$$\text{Normalized bandwidth} = (\omega_2 - \omega_1)/\omega_n \qquad (1.8)$$

The normalized bandwidth is the width of the resonant peak at 0.707 ($\sqrt{2}/2$) times the peak amplitude normalized by its associated resonant frequency (Figure 1.2). The stored energy is half its maximum value at this point.

(7) Internal Friction (Q^{-1}).

$$Q^{-1} = (\omega_2 - \omega_1)/\omega_n = 2\zeta \qquad (1.9)$$

The normalized bandwidth is also known as the internal friction. It is analogous to the damping or energy loss in an electrical system [Ref. 18:p. 445].

(8) Quality Factor (Q).

$$Q = \omega_n/(\omega_2 - \omega_1) \qquad (1.10)$$

The quality factor is the inverse of the normalized bandwidth. It is a measure of the sharpness of the resonant peak [Ref. 15:p. 76].

8
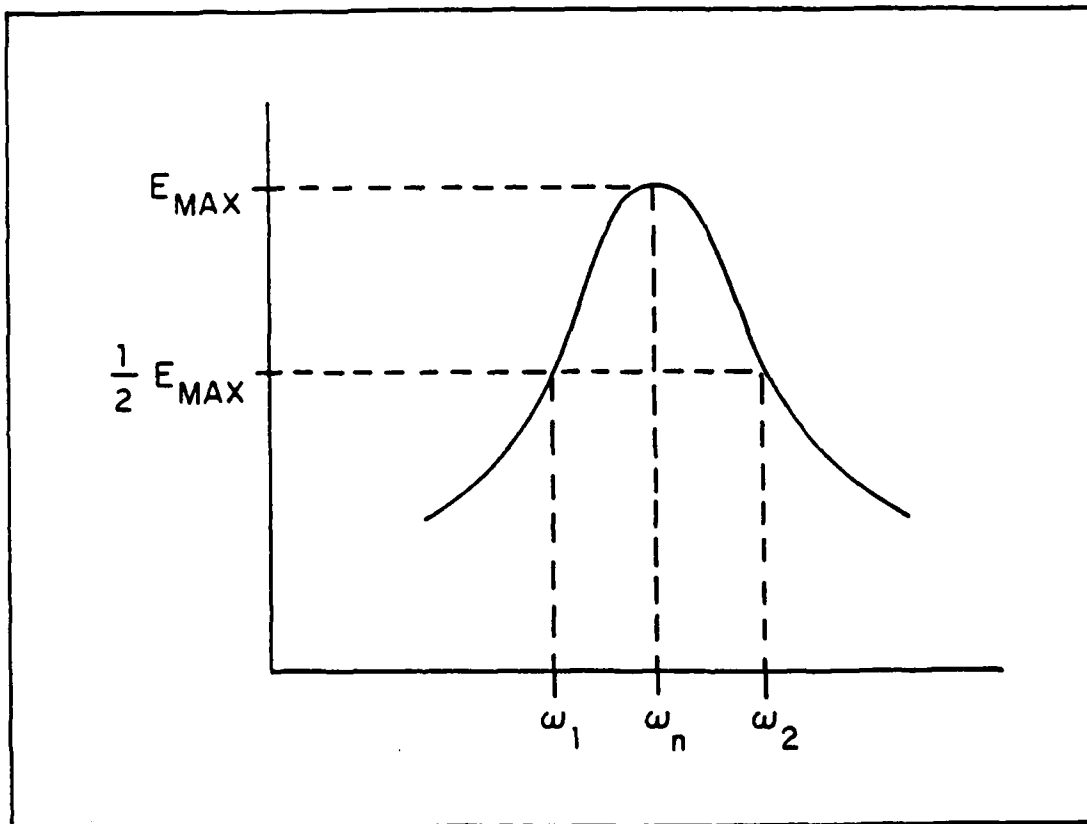
Figure 1.2   Normalized Bandwidth

(9) Phase Angle (α).

$$\tan \alpha \;=\; (1/\pi)\,\ln(a_i/a_{i+1}) \tag{1.11}$$

The phase ange is the angle by which the strain lags behind the stress in cyclic loading. The tangent of the phase angle can be taken as an index of energy loss [Ref. 15:p. 495]. If damping is small, i.e., ($\zeta \ll 0.5$), then,

$$\tan \alpha \;=\; \delta/\pi \;=\; Q^{-1} \;=\; 2\zeta \tag{1.12}$$

(10) Specific Damping Capacity (SDC) [Ref. 18:p. 444].

$$SDC \;=\; (a_{i+1}^2 - a_i^2)/a_i^2 \tag{1.13}$$

Again if ($\zeta \ll 0.5$), then

$$SDC(\%) \;=\; 200\pi Q^{-1} \tag{1.14}$$

(11). Resonant Frequency (ω_n).

$$\omega_n \;=\; (\beta_n \ell)^2 (EI/m\ell^4)^{1/2} \tag{1.15}$$

This is the natural frequency of the nth mode of a cantilever beam [Ref. 15:p. 464], where:

10

E = Young's Modulus of Elasticity

I = moment of Inertia

m = mass density per unit length

ℓ = vibrating length of the beam

$\beta_n\ell$ = values for several vibration modes (n) for a clamped-free beam. [Ref. 15:p. 466]

n	$\beta_n\ell$	$(\beta_n\ell)$
1	1.8751	3.5160
2	4.6941	22.0345
3	7.8548	61.6972

b. Measurement Method

Damping measurements in Fe-Cr-based alloys have been made with an inverted pendulum apparatus or a cantilever beam; usually under free decay conditions [Refs. 9-11,19]. A cantilever beam method was developed by Bolt, Beranek, and Newman, Inc., known as the single cantilever beam resonant dwell method [Ref. 20]. It is used to determine stress and frequency dependence of material damping over a frequency range of 25-1,000 Hz. The method indirectly determines the loss factors of simple structural elements by measuring their response to excitation at modal frequency.

In this method, the simple structural element is a thin section cantilever beam clamped to a weighted bar. The bar is connected to a random vibration generator at one

11

end and a heavy support frame at the other. The vibration input is measured by an accelerometer on the clamp at the base of the sample. The system tip deflection (response) is measured by a microscope focused on the tip of the beam. The beam tip is illuminated by a stroboscope.

This method was modified by Professor Y.S. Shin of the Naval Postgraduate School, wherein the system response is measured by an accelerometer at the beam tip. The signals of the input and output accelerometers are compared by a spectrum analyzer to produce the system transfer function. Strain response of the beam is measured by a strain gage placed at the first nodal point of the beam. A sample specimen is illustrated in Figure 1.3.

2. Microstructural Damping

The microstructural effects and interactions within a material result in damping. The phenomena associated with high damping in cyclically stressed crystalline materials are:

a) dislocation damping

b) interphase boundary damping

c) phase change effects.

The primary mechanism of damping in ferromagnetic materials is the magneto-mechanical hysteresis effect, a type of interphase boundary damping, described by de Batiste [Ref. 8]. The application of a mechanical or magnetic stress causes the domains which are favorably aligned to the stress
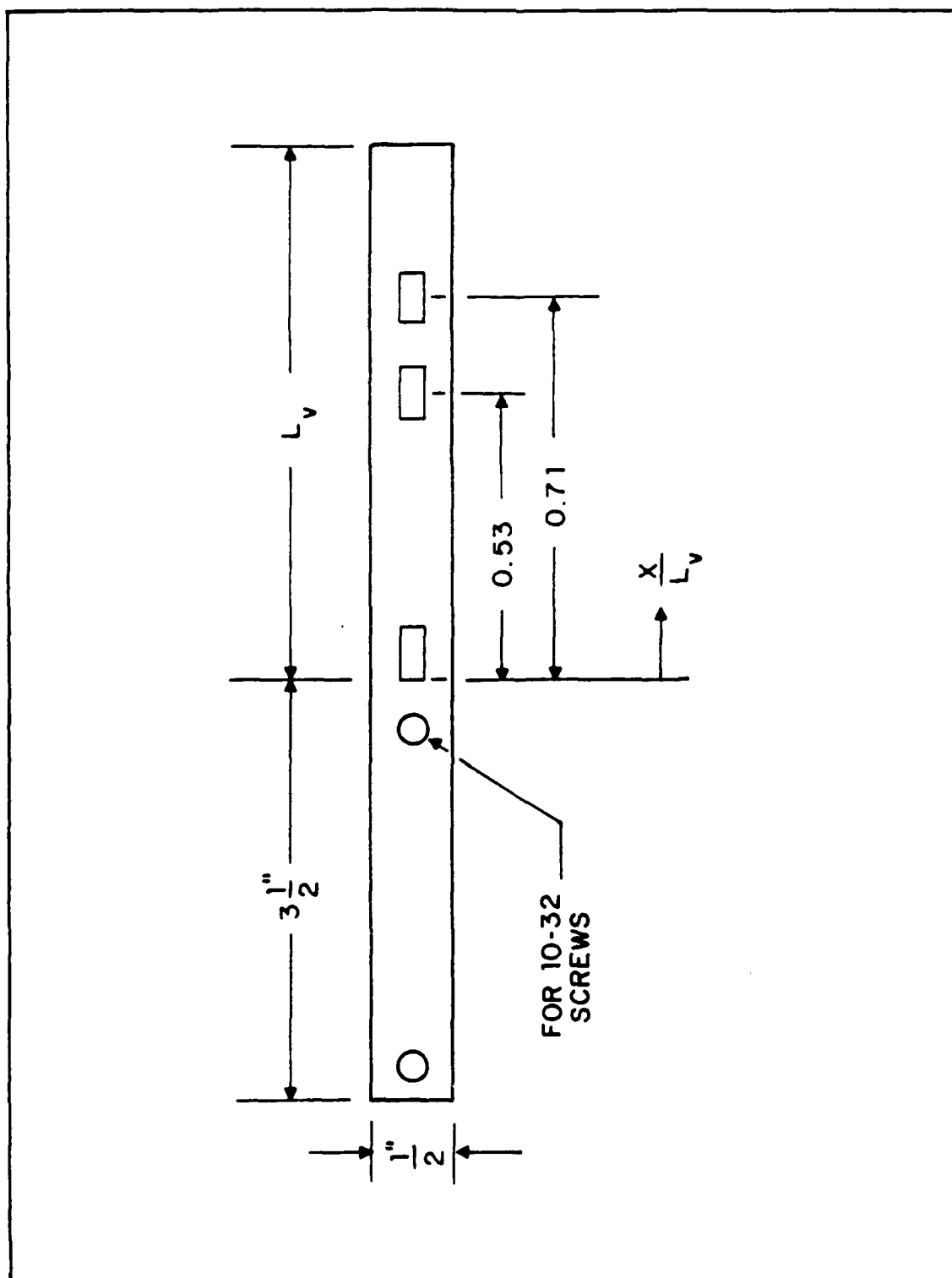
Figure 1.3   Specifications for Resonant Dwell
Method Damping Specimens

13

to grow preferentially to those domains not so favorably aligned. An increase in stress may cause a rotation of the magnetic moment vector within the domains toward the stress direction. Both effects increase the net magnetic moment of the sample [Ref. 18].

If the stress is supplied by an external force, the energy is used to rotate the domains. Therefore it is not all transmitted, resulting in damping. Prestressing the sample may result in larger aligned domains that do not rotate under the given stress, in which case less external energy may be absorbed and damping is decreased.

E. METALLURGY OF THE IRON-CHROMIUM ALLOY SYSTEM

1. Physical Properties

Stainless steels are divided into three main classes: ferritic, austenitic, and martensitic. The high damping Fe-Cr-based alloys are closely related to ferritic stainless steels. Ferritic stainless steel consists of an Fe-Cr alpha (α) solid solution with a body centered cubic (bcc) crystal structure. The alloy contains very little dissolved carbon, mostly as finely divided chromium carbide precipitates. The chromium content varies from about 12 to 30 weight percent. The alloy remains ferritic (bcc) up to the melting point [Ref. 21:p. 5-2].

The binary Fe-Cr phase diagram (Figure 1.4) shows a so-called gamma (γ) loop extending from about 0 to 12% chromium and temperatures from 850°C to 1400°C.

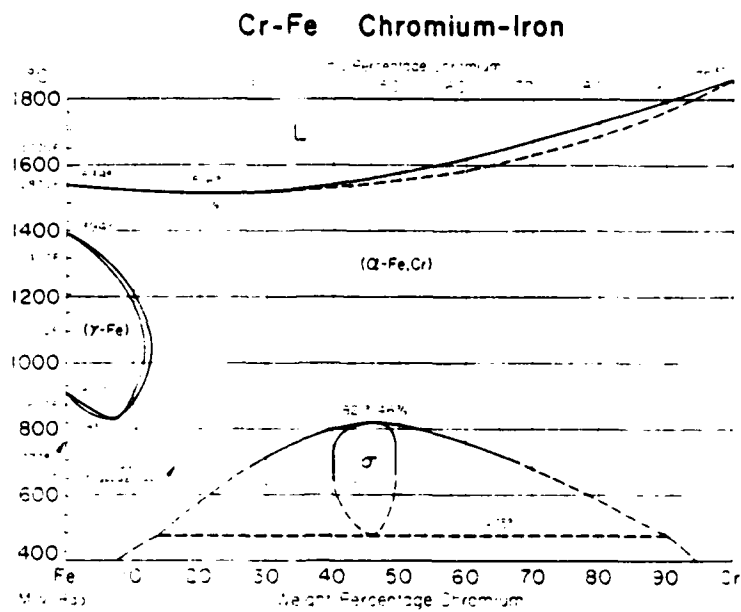## Cr-Fe   Chromium-Iron

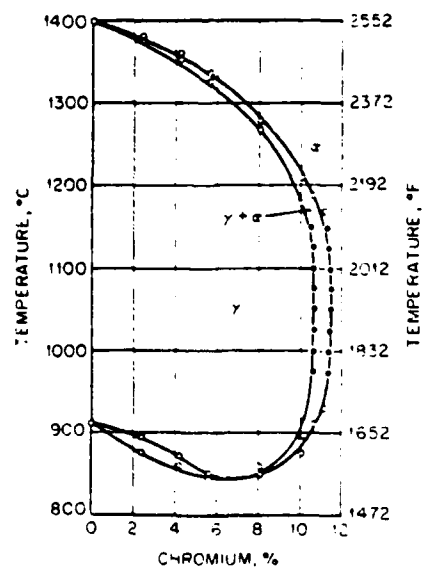Figure 1.4   Fe-Cr Binary Phase Diagram

Figure 1.5   The Gamma Loop of the Fe-Cr Phase Diagram

15

When the alloy coordinates are moved to within the gamma loop the alloy undergoes a phase change to the face centered cubic (fcc) form. An expanded view of the gamma loop is shown in Figure 1.5. The gamma loop is separated from the alpha region by a narrow two-phase band. The size, shape, and extent of the gamma loop can vary considerably with the proportions of ferritic stabilizing elements (such as chromium) and austenitic alloying elements (such as carbon and nitrogen) [Ref. 21:p. 5-2].

A three-component phase diagram for Fe-Cr-Mo is shown in Figure 1.6. Here we may notice that several intermetallic phases are possible. The most significant of these is the chi (χ) phase; a cubic structure of approximate composition $Fe_{36}Cr_{12}Mo_{10}$ or Fe_3CrMo [Ref. 22].

Some disadvantages of ferritic stainless steels are their poor machinability, poor weldability, high notch sensitivity and their susceptibility to embrittlement. The advantages of ferritic stainless steels include good damping properties and good corrosion resistance. Some of the corrosion resistance and ductility are lost after exposure to high temperatures, but this can be alleviated somewhat by alloying with molybdenum.

2. Damping Properties

The primary mechanism of damping in ferromagnetic alloys is associated with magneto-mechanical hysteresis
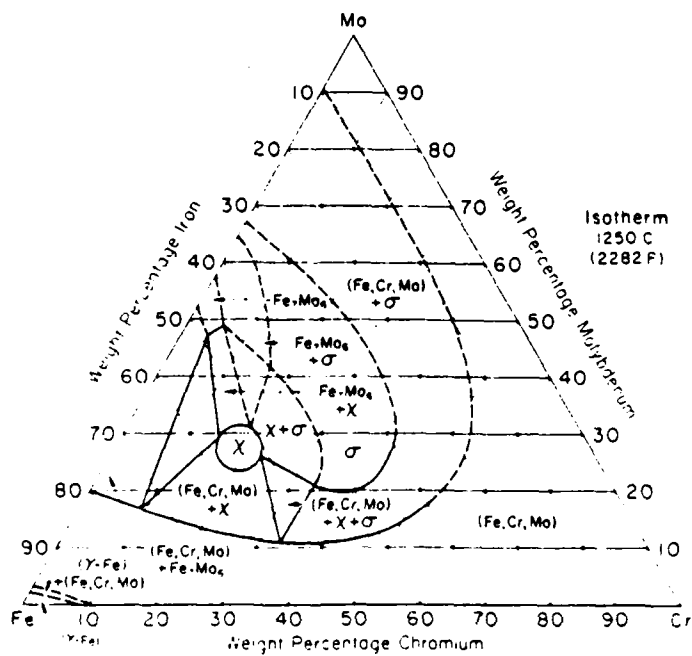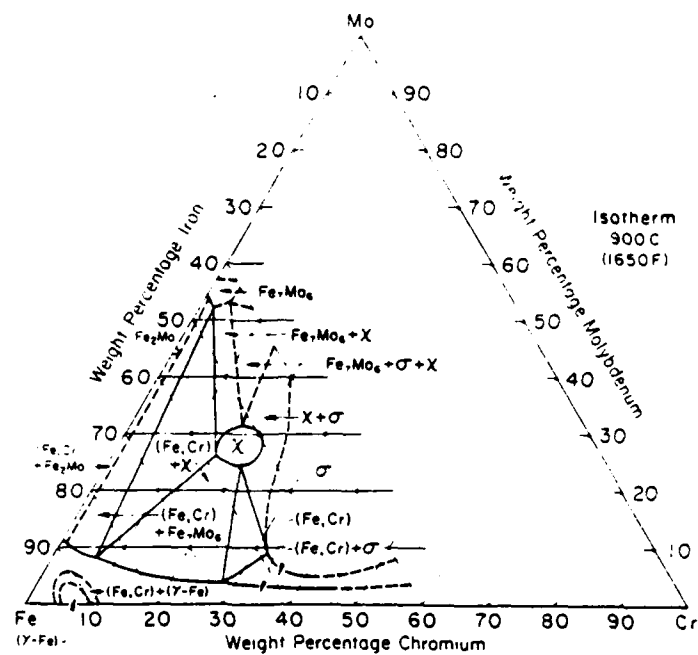
Figure 1.6   Ternary Phase Diagram for Fe-Cr-Mo
(a) 900°C Isotherm and (b) 1250°C Isotherm

17

(domain boundary) damping. In this, the inhibition of motion of the domain walls is the determinant of damping capacity and factors that affect the domain wall mobility will directly affect the damping capacity.

A temperature increase reduces magnetic permeability. Heating above the critical (Curie) temperature results in a random orientation of the domain boundaries and a transformation of the material from ferromagnetic to paramagnetic. This was originally considered to be a beta (β) phase of iron, but since the structure remains body centered cubic throughout this range, it is now considered a transformation within the alpha (α) phase [Ref. 18:p. 455].

The amplitude of applied strain also affects the damping capacity, causing an increase to a maximum value. Beyond that value, increasing stress will cause a decrease in damping.

Residual stresses that block domain mobility will tend to adversely affect damping capacity. Schneider, et al. [Ref. 12], report that, "damping capacity is strongly deteriorated by cold work. A reduction of $\geq$ 5% completely destroys the damping effect; however, it can be fully restored by a succeeding heat treatment."

Magnetic fields cause preferential growth of the domain walls along the line of the applied field. The domain walls become progressively less mobile with

increasing field strength and the damping capacity of the material is correspondingly reduced. Damping capacity disappears at magnetic saturation at about 100 A/cm [Ref. 12].

II. EXPERIMENTAL PROCEDURE

The David W. Taylor Naval Ship R&D Center (NSRDC), Annapolis, Maryland supplied partial ingots from two different Fe-Cr-based alloys. The ingot sections as provided were approximately 12.75 in. x 3.5 in. x 1.625 in. Bulk analysis, supplied with the ingots, was performed by Luvak Inc. of Boyleston, Ma. (Report number 0-1500): Their findings are presented in Table 1.

Dilatometer samples were machined from the ingots in accordance with Reference 23, Section IV. The tests were conducted on an Orton Automatic Recording Dilatometer Model 15 BC-1. All tests were performed in a flowing argon gas atmosphere.

Tensile specimens were machined from the ingots as per Reference 24. The tests were performed on an Instron Universal Testing Instrument Model TT-D. Specimens were tested to fracture directly or were subject to cyclic loading. The load on the cyclic samples was increased in steps until plastic deformation occurred. Then the samples were pulled to fracture. All samples were tested at room temperature at strain rates of 0.641×10^{-3} sec^{-1}.

Damping specimens were machined to the specifications of the modified Resonant dwell technique [Ref. 20]. Strain

TABLE 1

BULK ANALYSIS OF ALLOYS (WT%)

Element	Sample 1	Sample 2
Fe	84.9	84.7
Cr	11.61	11.7
Mo	–	2.92
Al	2.89	0.002
C	0.007	0.006
N	0.0011	0.0009
O	0.0019	0.020
S	0.004	0.005
Ni	0.006	0.006
B	0.002	0.002
Ca	0.0018	0.0016
Si	–	0.011
Remainder	0.576	0.626

gages were attached at the three model points (Figure 1.3). Specimen dimensions are listed in Table 2.

The various specimens were annealed for one hour in a Lindberg Hevi-Duty Type 54253 tube furnace, at temperatures of 950°C, 1000°C, 1050°C, and 1100°C. All specimens were annealed and furnace cooled under flowing argon gas. The samples were stored at room temperature.

A new testing apparatus was developed and used for the damping capacity measurements. This apparatus was based on a Spectral Dynamics SD-380 Signal Analyzer providing a 40 kHz broadband noise signal to an MB Dynamics Inc. Model 2125MB amplifier which then drove an MB Dynamics Inc. Model PM-25 Vibration Exciter. The PM-25 oscillated an instrumented cantilever beam specimen. One end of the beam was free and one was clamped. Acceleration of the beam base and tip were provided to the SD-380 Signal Analyzer by two Endevco Model 2250A-10 accelerometers via Endevco Model 4416A signal conditioners.

Strain measurement was provided to the SD-380 Signal Analyzer by Measurements Group Inc. strain gages (model CEA-13-250UN-350) via a Measurement Group Inc. bridge amplifier meter (BAM-1). The BAM-1 and the SD-380 were calibrated to give a direct reading of microstrains.

The interference to mode one excitation low strain frequency response reported in References 2 and 6 was also

TABLE 2

SDC SPECIMEN DIMENSIONS

Heat Treatment	Thickness (in)	Width (in)	Vibrating Length (in)
Fe-Cr-Al			
1100	0.083	0.503	7.02
1050	0.083	0.502	7.03
1000	0.081	0.502	7.03
950	0.803	0.504	6.87
Fe-Cr-Mo			
1050	0.084	0.508	7.02
1000	0.084	0.512	7.03
950	0.084	0.506	7.01

noticed here. The amplifier as well as the shaker may be contributing to this.

A block diagram of the system is given in Figure 2.1.

In some of the following figures reference is made to test specimens by their local designations which are as follows:

The first letter indicates the material; A--aluminum (Fe-Cr-Al) or M--molybdenum (Fe-Cr-Mo).

The second letter indicates the sample usage; T--tensile specimen, D--dilatometer sample, B--SDC beam, etc.

The number in the third position is the number of the sample. For example: AT-4 is the fourth tensile sample of Fe-Cr-Al, and MB-2 is the second SDC beam of Fe-Cr-Mo.
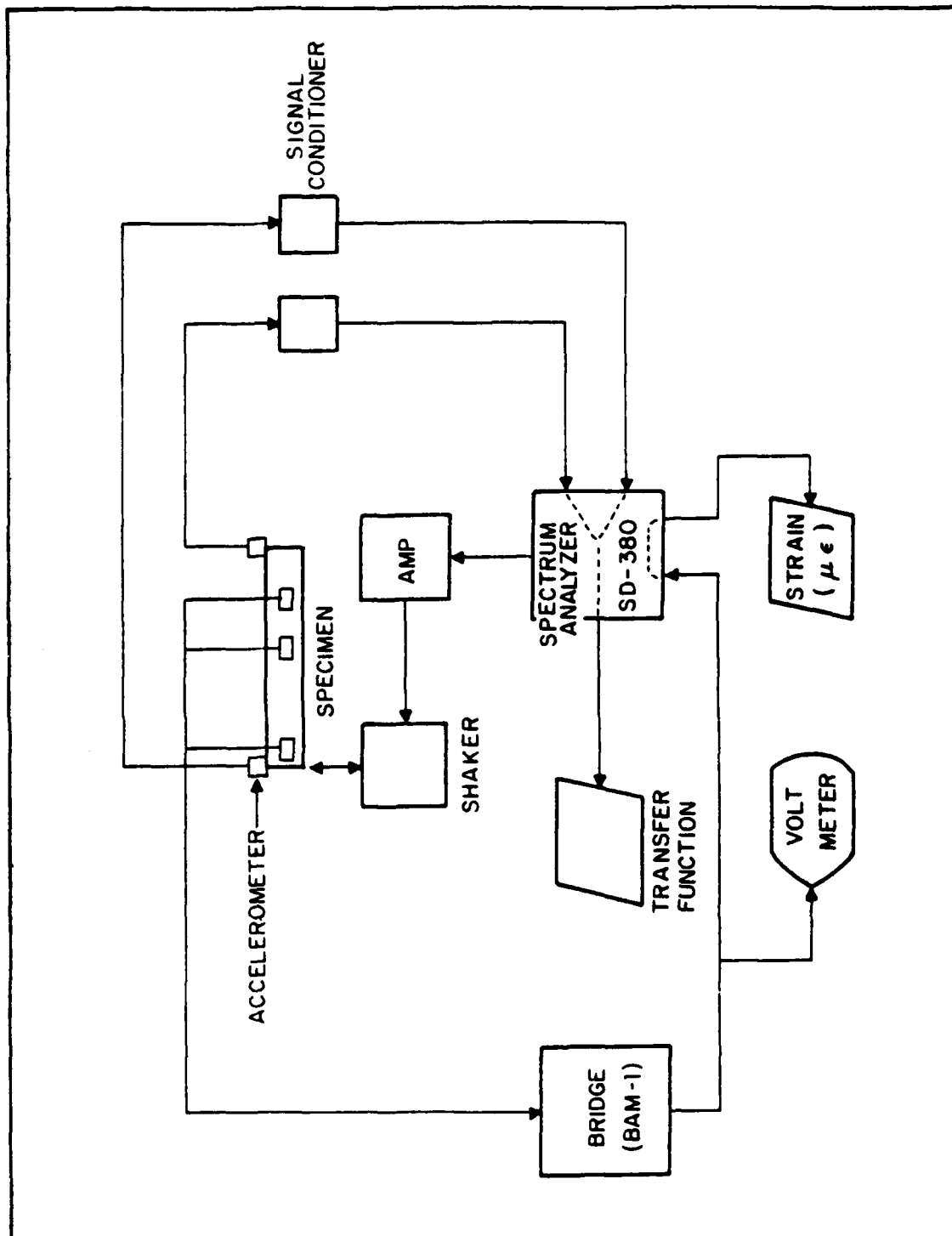
Figure 2.1 Damping Capacity Testing Block Diagram

25

III. RESULTS AND DISCUSSION

A. DILATOMETRY

In a previous study of an Fe-Cr-Mo alloy by O-Toole, an unusual variation in damping properties for a 1000°C anneal/furnace cooled specimen was noticed when compared to the same alloy when annealed at other temperatures. In particular, SDC was less than expected and tensile properties were higher. It was postulated that the difference might be due to a phase change taking place, perhaps related to an interaction with the gamma loop (see the Fe-Cr phase diagrams, Figures 1.4, 1.5) or perhaps due to the intermetallic chi phase (see the ternary Fe-Cr-Mo diagram, Figure 1.6). Optical examination by O'Toole showed what could be some slight second phase formation at the grain boundaries of furnace cooled specimens (absent in water-quenched specimens). This second phase was assumed to be the chi (χ) phase. However, no direct correlation between this sort of microstructure and damping capacity was determined, and O'Toole recommended further investigation, such as via dilatometry [Ref. 6].

Dilatometric investigation in the present work showed a slight change in slope at about 750°C, but certainly not the characteristic "notch" in the length vs. temperature plot which would indicate a distinct phase change. A typical

26

dilatometric plot (for the Fe-Cr-Al alloy) is shown in Figure 3.1. A similar slope change is seen for the Fe-Cr-Mo sample (Figure 3.2). For comparison purposes, the plot for a sample of pure iron is presented in Figure 3.3, wherein an obvious phase change occurs in the vicinity of 910°C, as predicted in the equilibrium phase diagram (Figure 1.4).

Various dilatometric scans were performed with variations in the following parameters: heat treatment, heating rate, cooling rate and soaking time at maximum and intermediate temperatures. In all cases the results closely followed those illustrated, with no distinct evidence of a phase change over the temperature range scanned (18°C–1100°C).

B. TENSILE TESTING

1. Tests to Fracture

The method of tensile testing to failure used by O'Toole [Ref. 6] was modified to accommodate the tendency of these rather large-grained Fe-Cr-based alloys to fail to break cleanly under load. The large-grained samples tend to develop a mottled, dimpled appearance at the onset of necking, and further loading typically produces longitudinal cracks. These cracks separate into individual longitudinal strands with a cable-like appearance, and the individual strands then break in sequence. The resultant stress strain curves show a long slow decline after necking punctuated by vertical dips as each strand breaks, and the
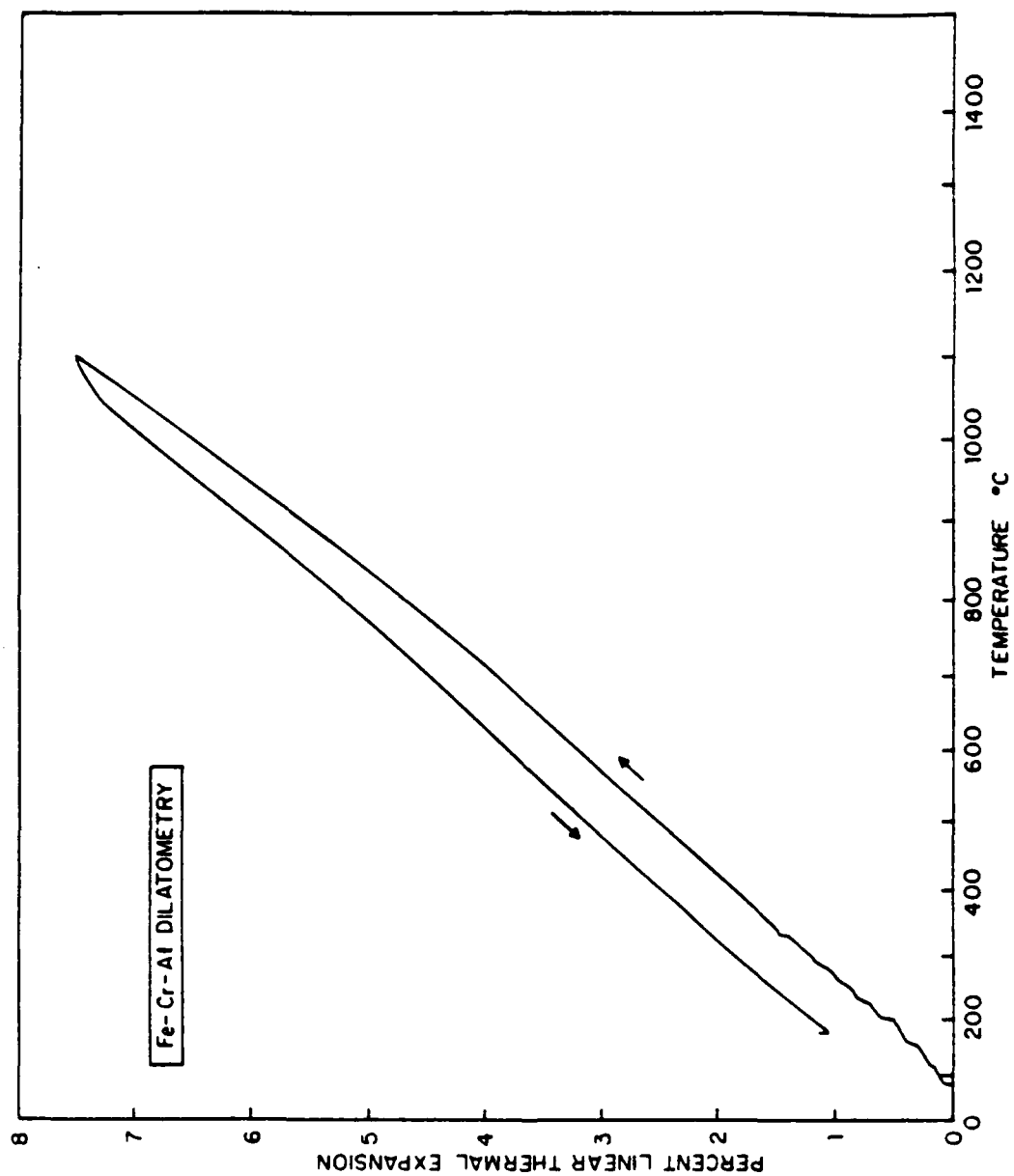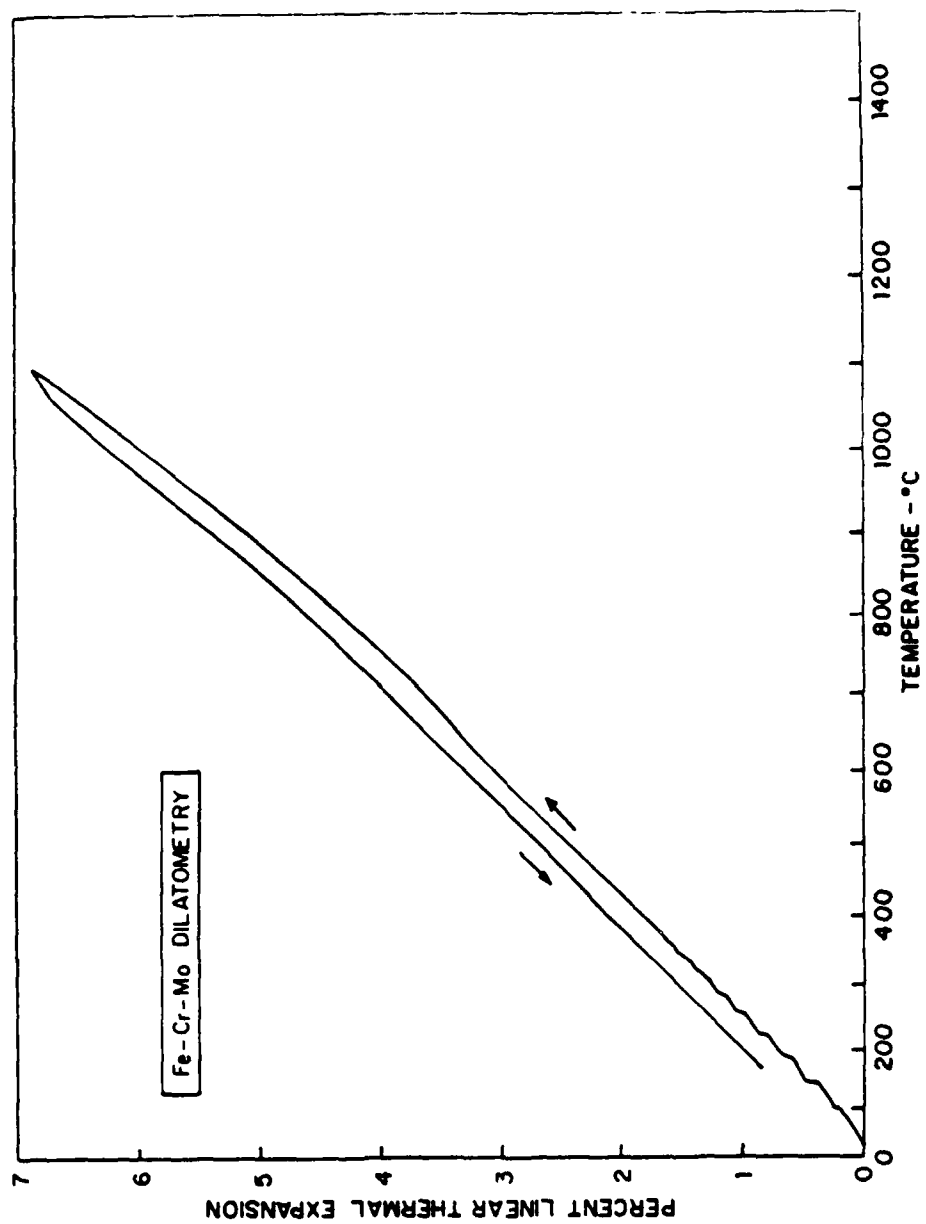
27

Figure 3.1 Fe-Cr-Al Dilatometry

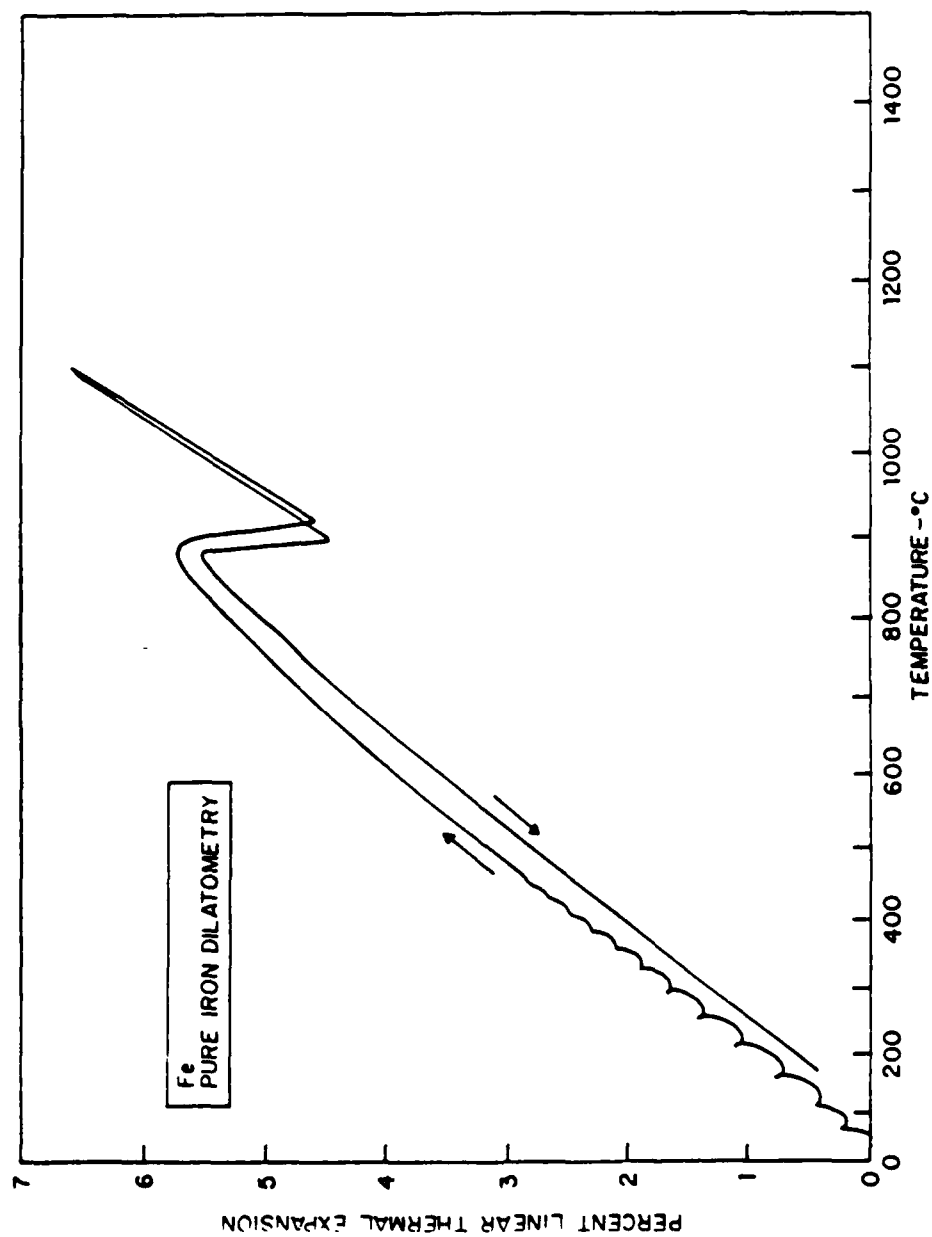Figure 3.2 Fe-Cr-Mo Dilatometry

29

Figure 3.3   Iron Dilatometry

30

stress level nearly reaches zero before the final strand parts.

In order to eliminate the maximum elongation error due to these effects, the final fracture point on all curves was arbitrarily taken to be at a strain (beyond necking) corresponding to 0.75 times the ultimate tensile strength (UTS). The resulting stress-strain curves are presented in Figures 3.4, 3.5, and 3.6 and the strength vs. ductility data are presented in Table 3. Ductility was measured by taking 100 times the charted strain distance (the distance from the tangent to the elastic slope of the curve to the point of 0.75 times the tensile strength less the elastic portion of the curve) divided by the magnification factor (the chart speed divided by the cross-head speed) times the gage length.

$$\frac{e_{cf}}{mag \cdot \ell_o} \times 100 = \text{Ductility} \qquad (3.1)$$

As a comparison another measure of ductility, the percent elongation, was calculated using the standard gage length formula.

$$\frac{\ell_F - \ell_o}{\ell_o} \times 100 = \% \text{ elongation} \qquad (3.2)$$

As can be seen in Table 3, these methods agree quite closely for the aluminum samples, but not as well for molybdenum samples.
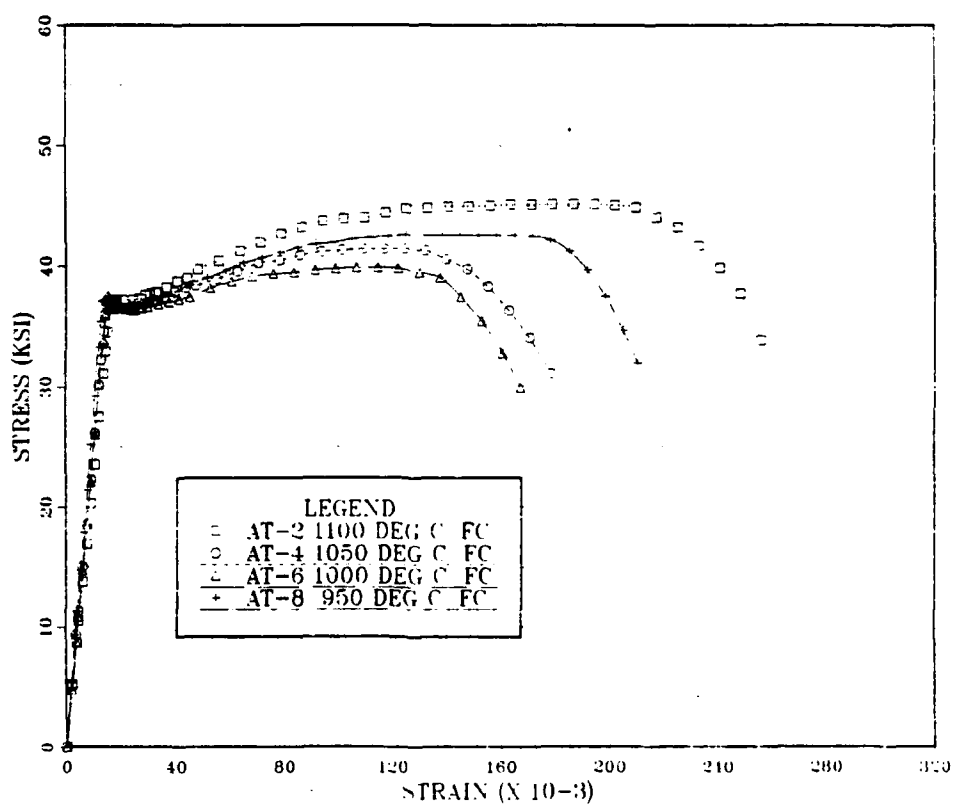
31

TENSILE TEST FE-CR-AL

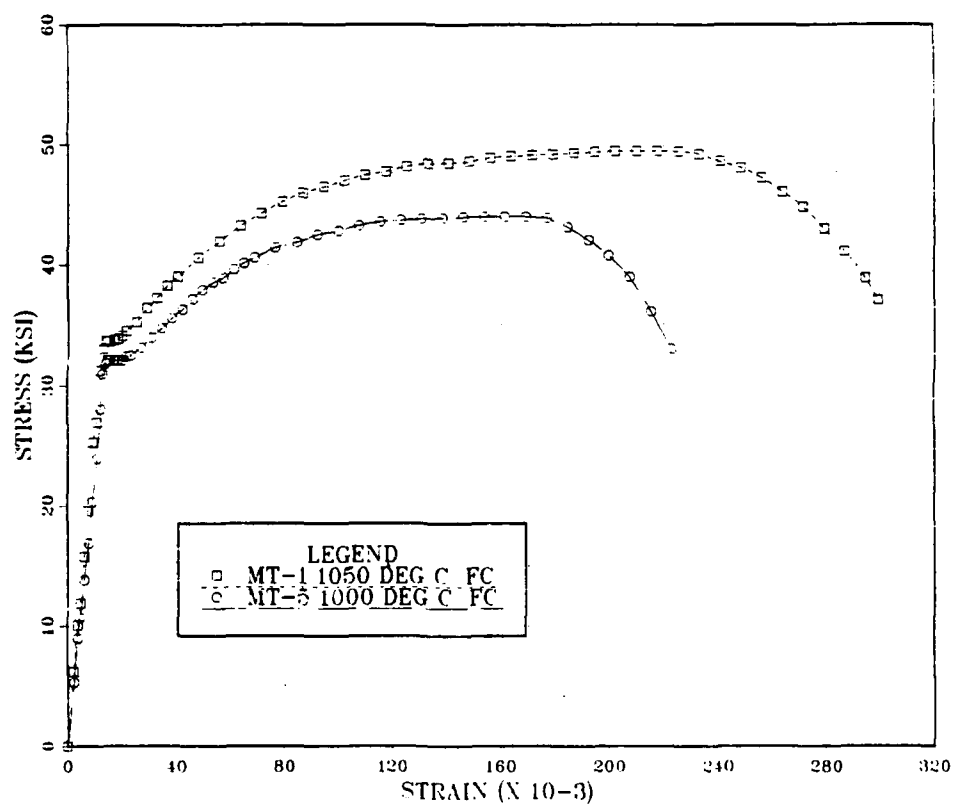
Figure 3.4   Fe-Cr-Al Tensile Test

TENSILE TEST FE–CR–MO

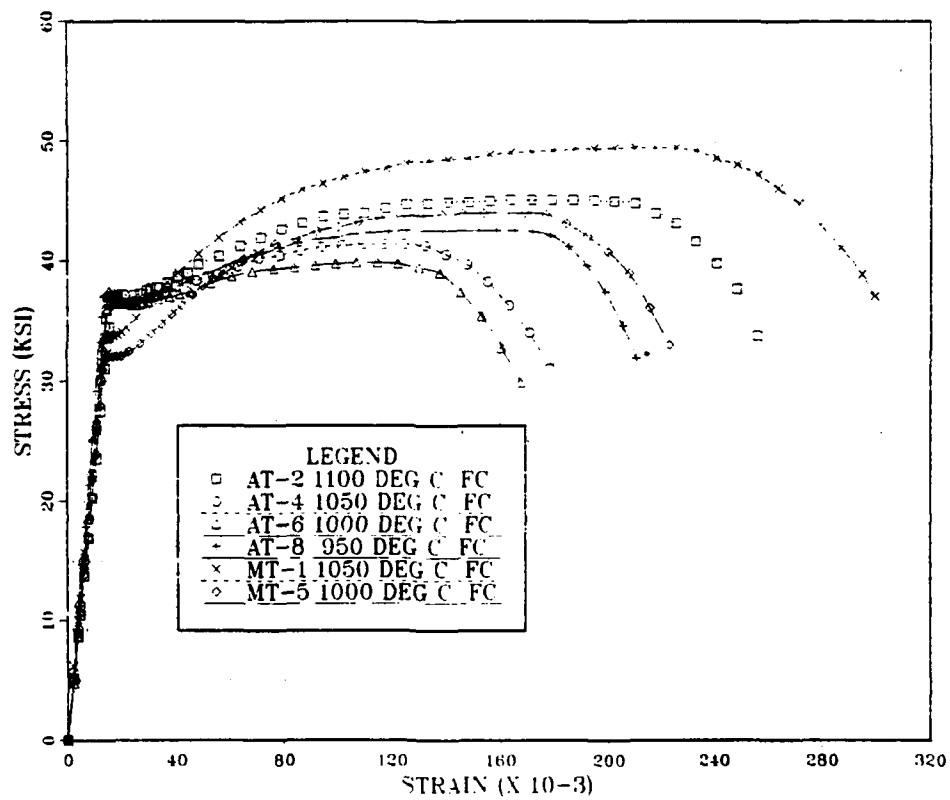Figure 3.5 Fe-Cr-Mo Tensile Test

33

TENSILE TEST FE-CR BASED ALLOYS

Figure 3.6   Fe-Cr-Based Alloys Tensile Tests

TABLE 3

STRENGTH AND DUCTILITY FROM TENSILE TESTS

Heat Treatment	Yield Strength (ksi)	UTS (ksi)	Ductility %	Elongation %
Fe-Cr-Al				
1100	37.18	45.12	24.12	26.15
1050	36.44	41.40	16.54	14.62
1000	37.54	39.88	15.46	16.92
950	37.15	42.57	19.93	19.33
Fe-Cr-Mo				
1050	33.66	49.44	28.43	36.15
1000	32.05	44.02	16.19	25.38

Of great interest was the elastic nonlinearity reported previously by O'Toole [Ref. 6]. This was noticed again in the present work and will be discussed in more detail later. However, for the purposes of simply showing the basic strength and ductility mechanical properties, the nonlinear portions of the curves, at low stress, have been omitted in the presentation of Figures 3.4-3.6. Since the nonlinearity was much more significant for the molybdenum samples, the figures in Table 3 would be in closer agreement if the nonlinear portion had been added to the charted strain distance (e_{cf}) in the ductility equation (Equation 3.1).

2. **Tensile Hysteresis Testing**

Low strain cyclic tensile hysteresis loading tests were conducted on representative specimens from each heat treatment. Each sample was alternately loaded to and un-loaded from 100, 250, 500, 750, and 1000 lbs in succession. Loading-unloading was continued in steps to 1500 and 2000 lbs until plastic deformation occurred. Once plastic defor-mation had commenced, the loading was continued until frac-ture. Distinct nonlinear "elastic" behavior was observed for both aluminum and molybdenum samples. Initially, these effects were suspected to be due to the imperfect stiffness and clearance in the specimen grips. In order to test this possibility, relatively larger steel samples were loaded and unloaded to 5000 lbs. In these a very minor degree of

36

nonlinearity was observed and it was determined that grip effects are saturated at a loading of only about 10 lbs (about 0.2 ksi stress). This could account for a portion of the low strain nonlinearity observed in the Fe-Cr-Al alloy samples, but for the Fe-Cr-Mo alloy samples, the behavior was much more complex.

For the Fe-Cr-Mo samples, the nonlinear region extends over a much wider range, corresponding to loads of about 75 lbs (stress of about 1.5 ksi). Roughly subtracting a proportion of this attributable to grip effects still leaves a significant degree of nonlinear response. In addition, all the Fe-Cr-Mo samples showed a sharp load drop followed by a gradual rise in this nonlinear elastic region. The load drop was repeated in subsequent loadings of a given sample. For this reason, and because the Fe-Cr-Al alloy samples did not display this load-drop phenomenon, it seems unlikely that this was due to the grips themselves (the grips are threaded). The load drop was observed only on loading, not on unloading.

The tensile hysteresis load-unload curves are presented in Figures 3.7-3.15. In these the vertical scale is in engineering stress (ksi) and the horizontal scale is relative strain (x 10^{-3}). The individual curves in the various load sequences are arbitrarily placed along this relative strain scale in order to provide a better means of comparison of the slope changes of the various curves. This

37
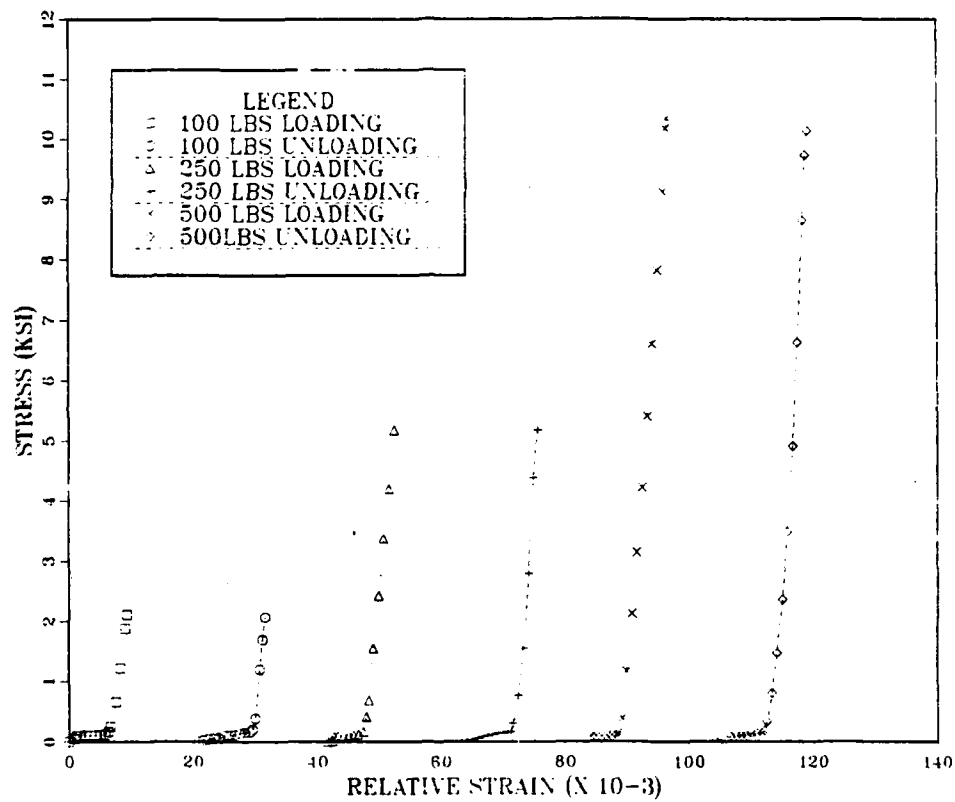
AT-1 1100 DEG C F.C.

Figure 3.7   Fe-Cr-Al 1100°C Tensile Hysteresis Test

38
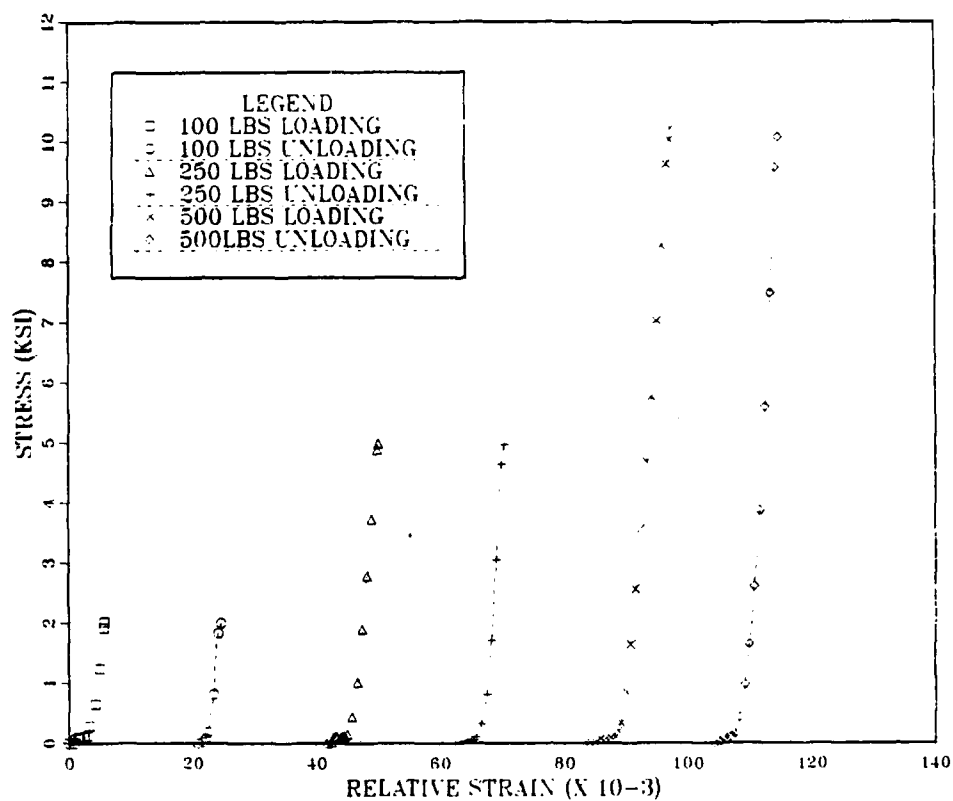
AT-3 1050 DEG C F.C.

Figure 3.8 Fe-Cr-Al 1050°C Tensile Hysteresis Test
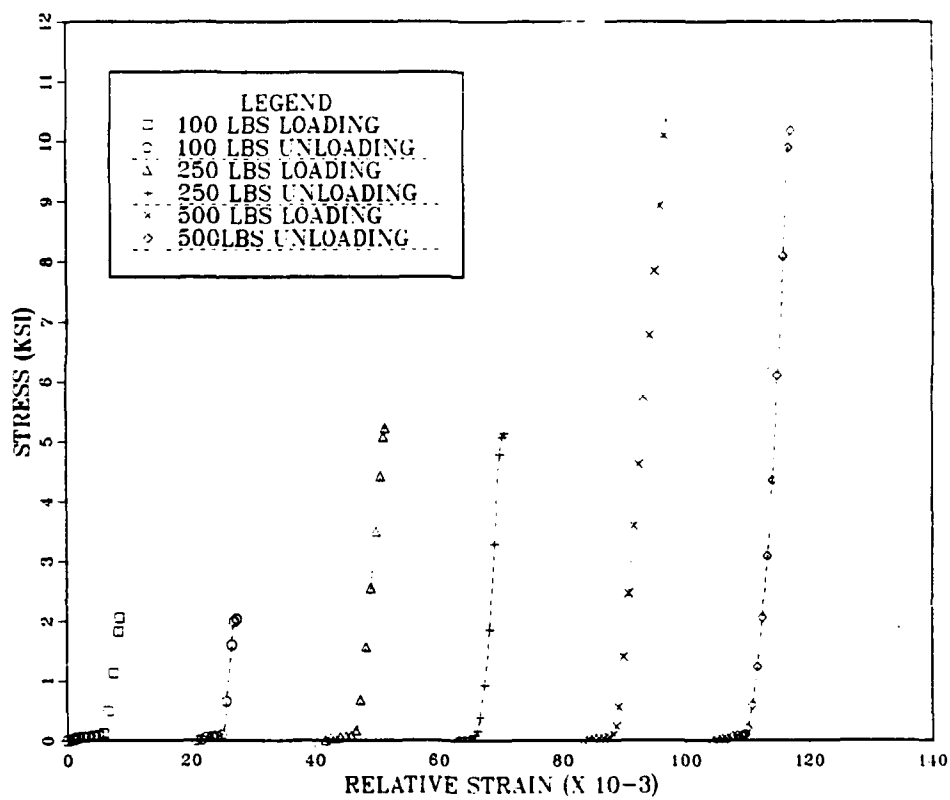
AT-5 1000 DEG C F.C.

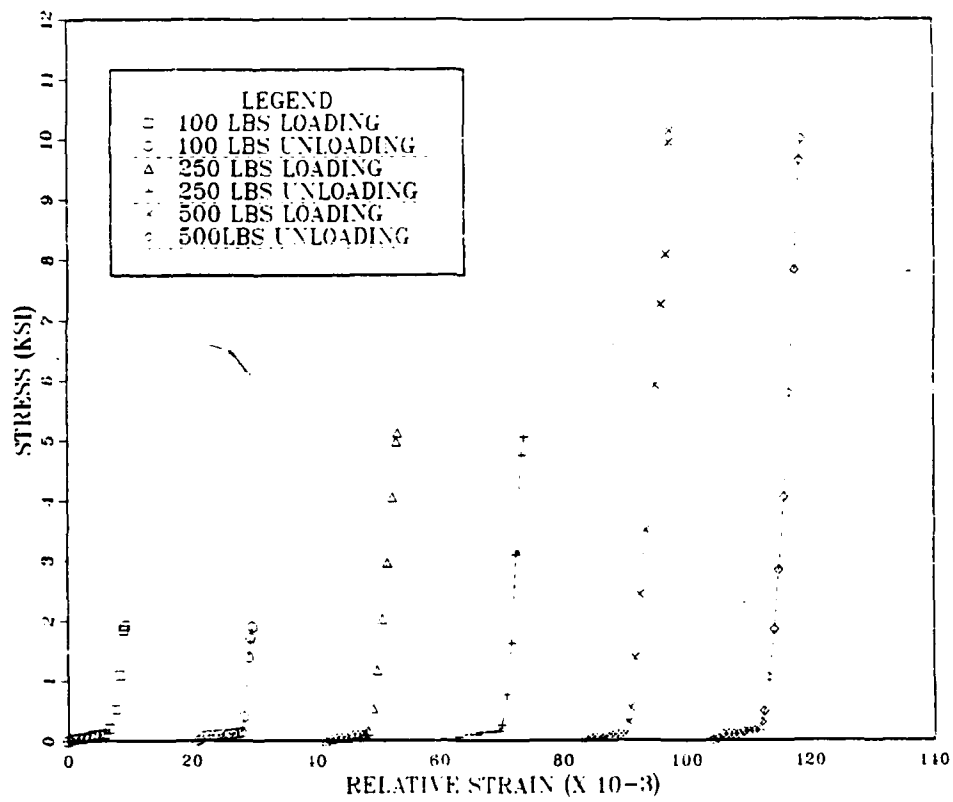Figure 3.9 Fe-Cr-Al 1000°C Tensile Hysteresis Test

AT-7 950 DEG C F.C.

Figure 3.10   Fe-Cr-Al 950°C Tensile Hysteresis Test
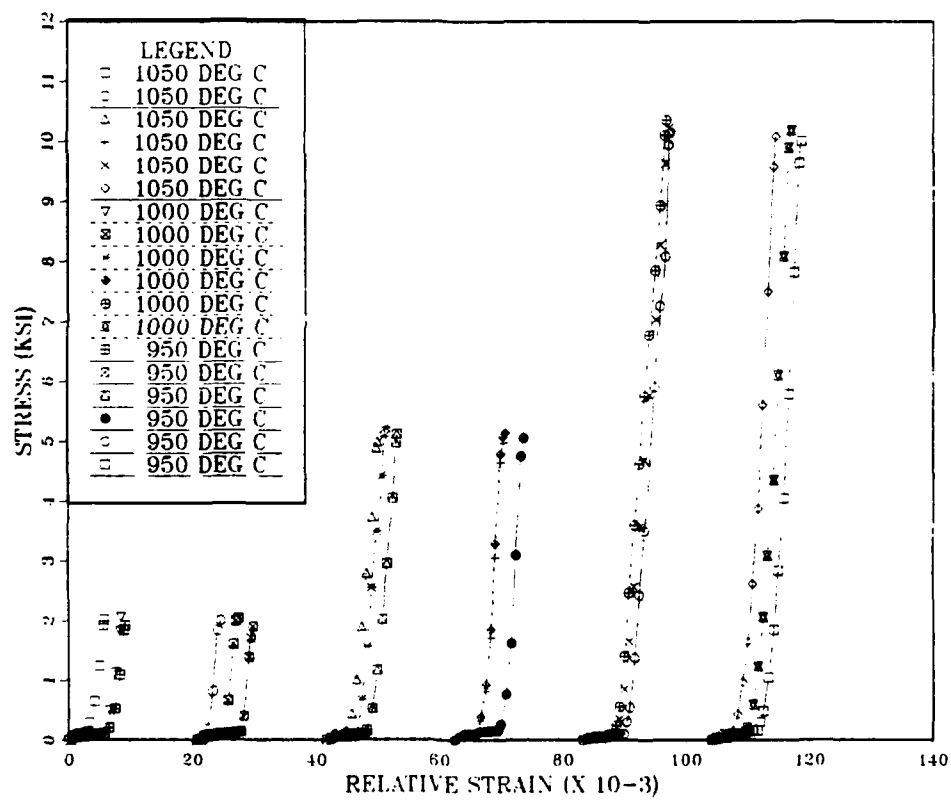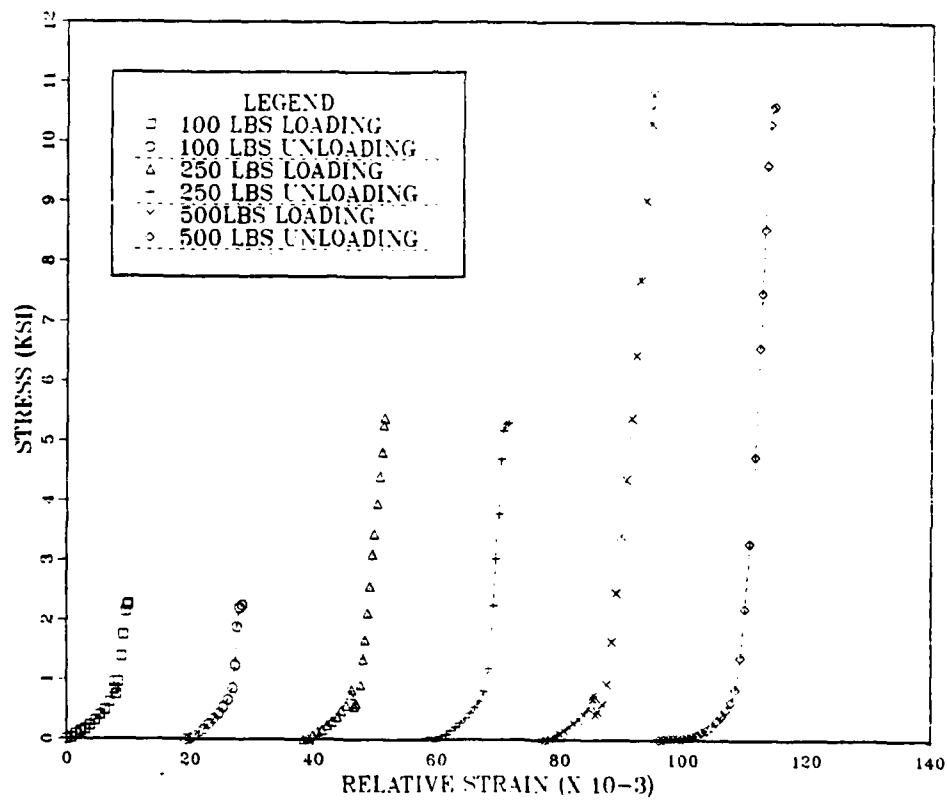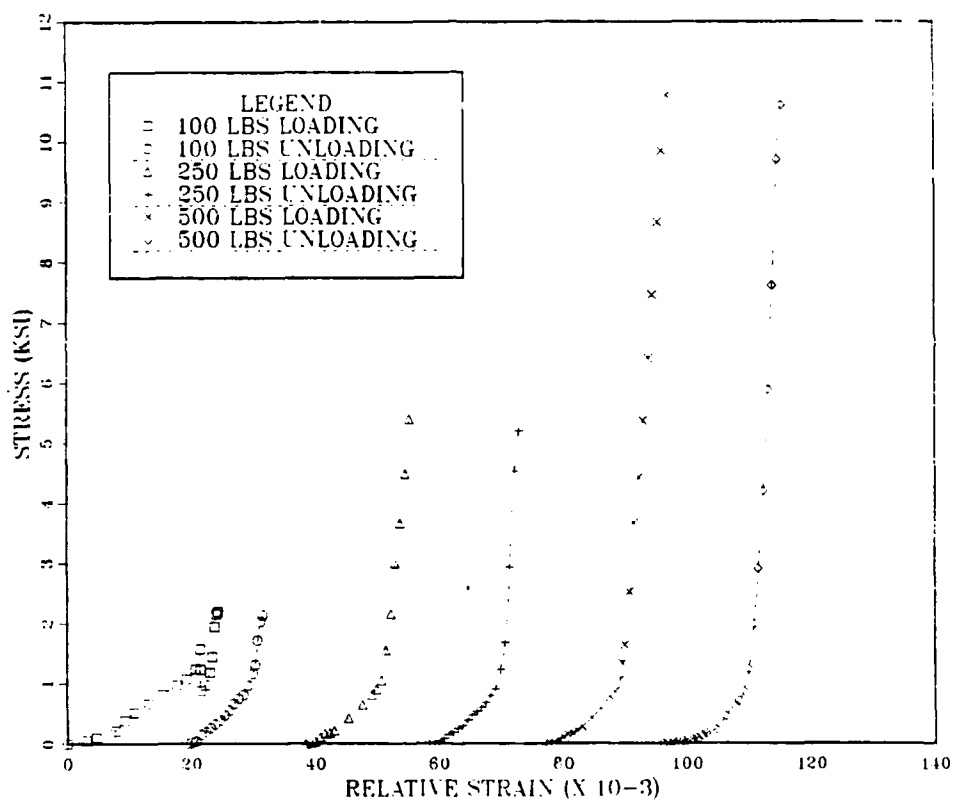
41

FE-CR-AL HYSTERESIS

Figure 3.11   Fe-Cr-Al Combined Tensile Hysteresis Tests

42

MT-2 1050 DEG C F.C.

LEGEND
- 100 LBS LOADING
- 100 LBS UNLOADING
- 250 LBS LOADING
- 250 LBS UNLOADING
- 500LBS LOADING
- 500 LBS UNLOADING

STRESS (KSI)

RELATIVE STRAIN (X 10-3)

Figure 3.12   Fe-Cr-Mo 1050°C Tensile Hysteresis Test

43

MT-4 1000 DEG C F.C.

Figure 3.13   Fe-Cr-Mo 1000°C Tensile Hysteresis Test

44

MT-7 950 DEG C F.C.
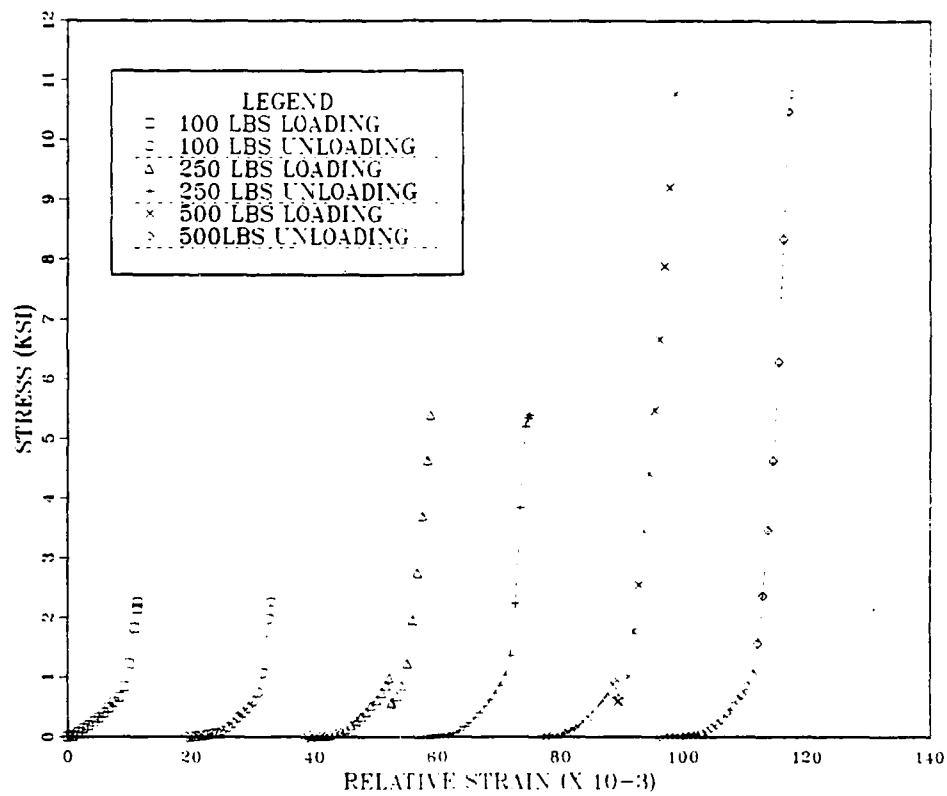
Figure 3.14   Fe-Cr-Mo 950°C Tensile Hysteresis Test

45

FE-CR-MO HYSTERESIS
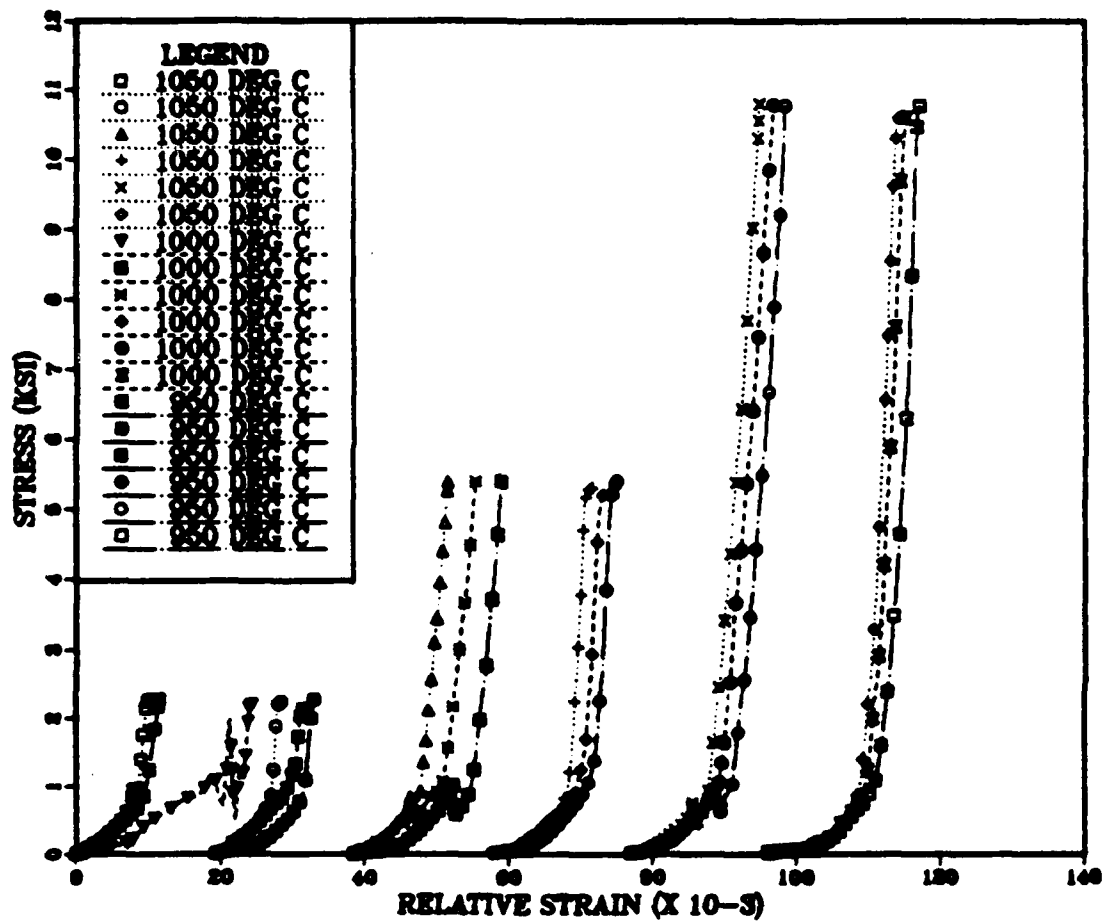
Figure 3.15   Fe-Cr-Mo Combined Tensile Hysteresis Tests

of course does not imply an actual strain offset between results from the various curves. However, on the plots where a set of variously heat-treated specimens are co-plotted, a direct strain comparison is possible for the curves which are originating from a common (relative) strain point. Once again, the points of origin (of the sets) were placed arbitrarily to separate the curves.

In interpreting the relative "resistance to strain" from these plots, we refer to the horizontal displacement of the near linear (near vertical) section from the point of origin, with higher "resistance to strain" corresponding to a smaller distance. Using that basis of comparison, the various samples have been ranked from higher relative resistance to lower relative resistance. These results are presented graphically in the figures and are summarized in Table 4.

Figures 3.7 to 3.15 also provide a comparison of the slopes of upper portions, showing that, in general the slope (modulus) increases with increasing stress.

Figures 3.16 to 3.336 were also derived from the tensile load-unload hysteresis tests. These figures have been contrived in order to provide a visual comparison of the slopes of the stress strain curves. Each line represents the slope of a tangent line to the stress strain curve near the maximum load point, indicated by the bold portion of the line. The bracketed, bold sections in these

TABLE 4

TENSILE HYSTERESIS TESTS--RESISTANCE TO STRAIN
(Ranked from High Resistance to Low Resistance)

100 lbs Loading	100 lbs Unloading	250 lbs Loading	250 lbs Unloading	500 lbs Loading	500 lbs Unloading
Fe-Cr-Al					
1050	1050	1050	1050	1000	1050
1000	1000	1000	1000	1050	1000
950	950	1100	950	1100	950
1100	1100	950	1100	950	1100
Fe-Cr-Mo					
1050	1050	1050	1050	1050	1050
950	1000	1000	1000	1000	1000
1000	950	950	950	950	950
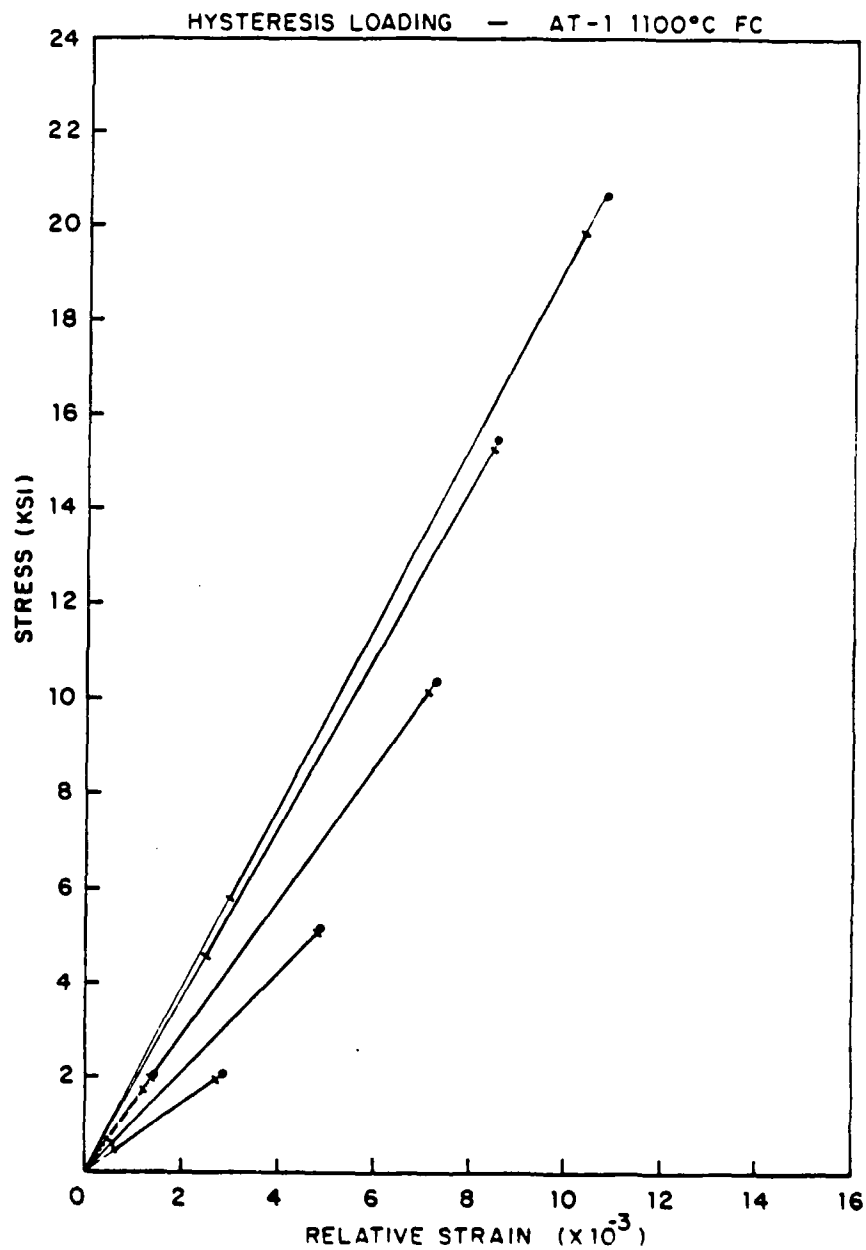
Figure 3.16   Fe-Cr-Al 1100°C Tensile Hysteresis Loading Slopes
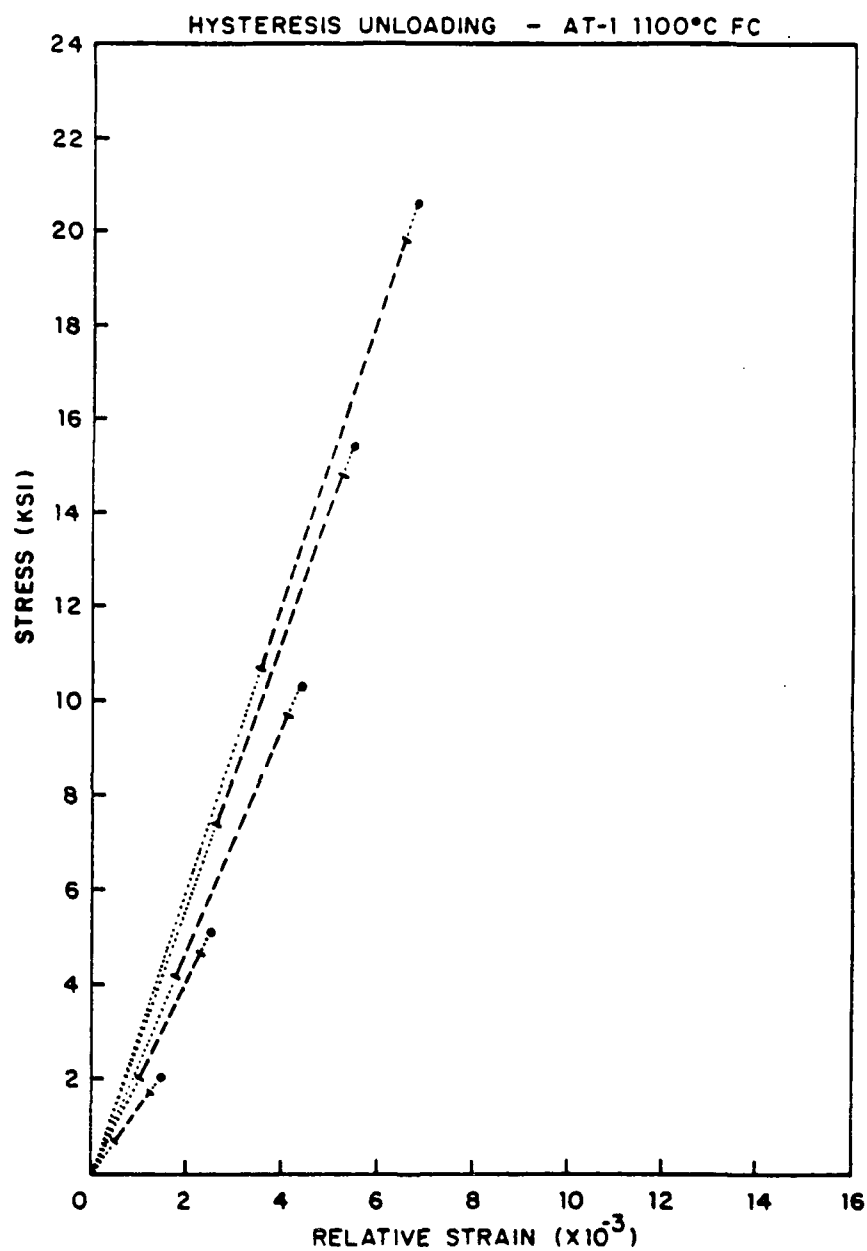
Figure 3.17   Fe-Cr-Al 1100°C Tensile Hysteresis
Unloading Slopes

50
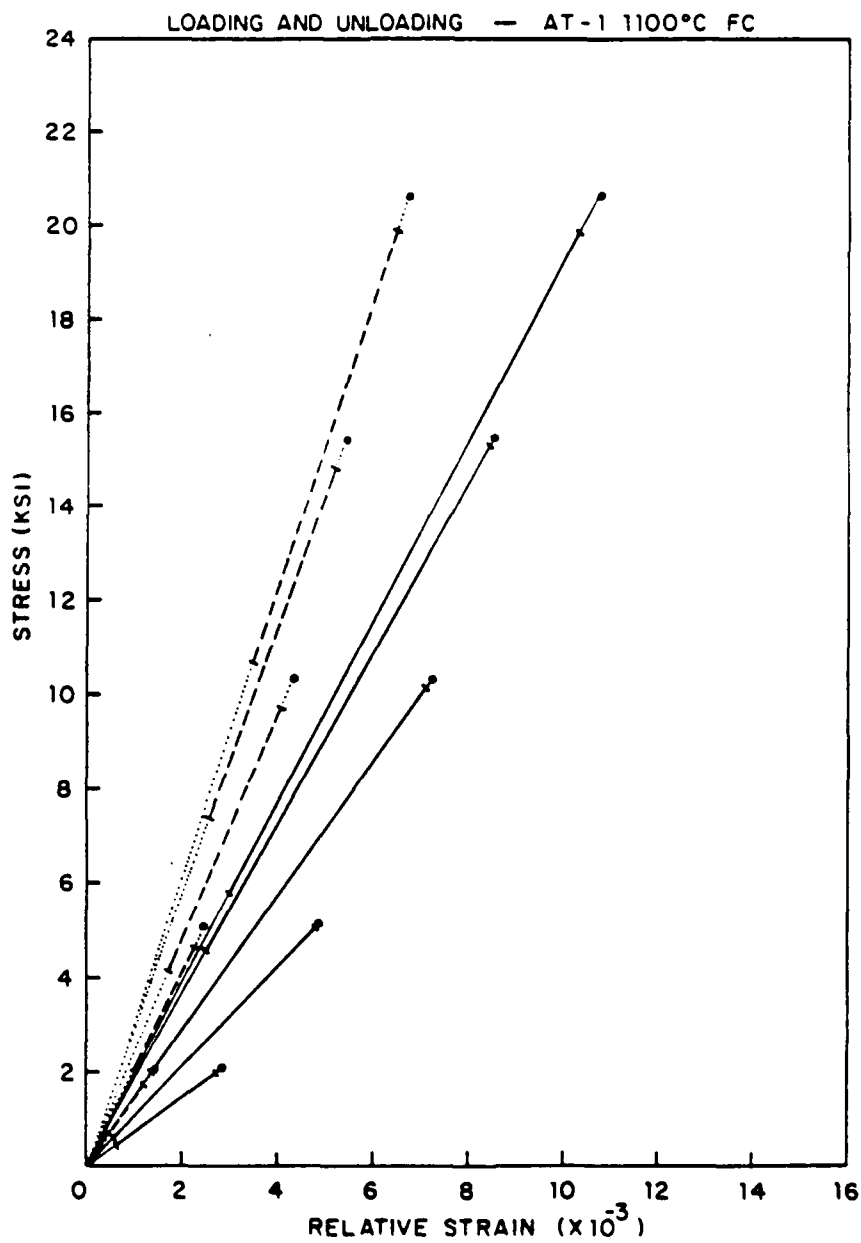
Figure 3.18   Fe-Cr-Al 1100°C Combined Tensile
Hysteresis Slopes

51
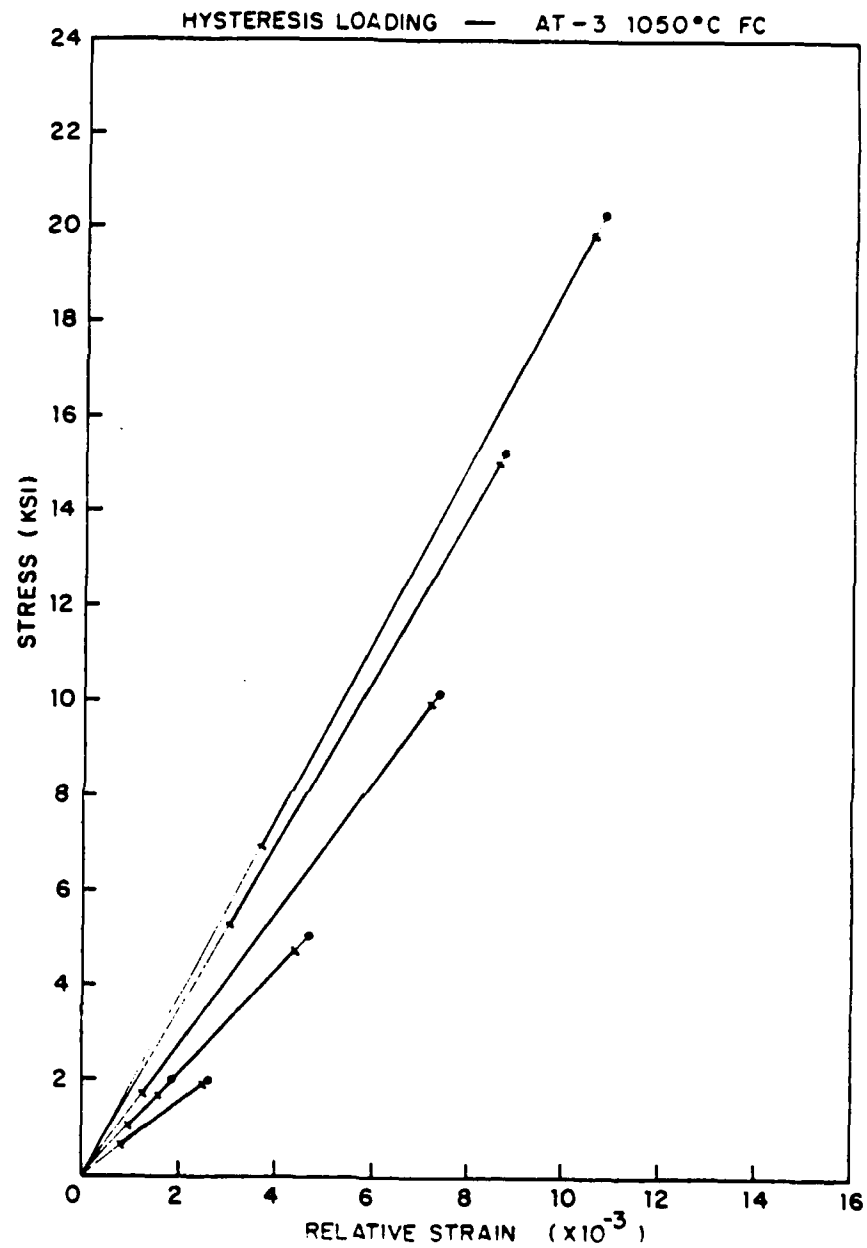
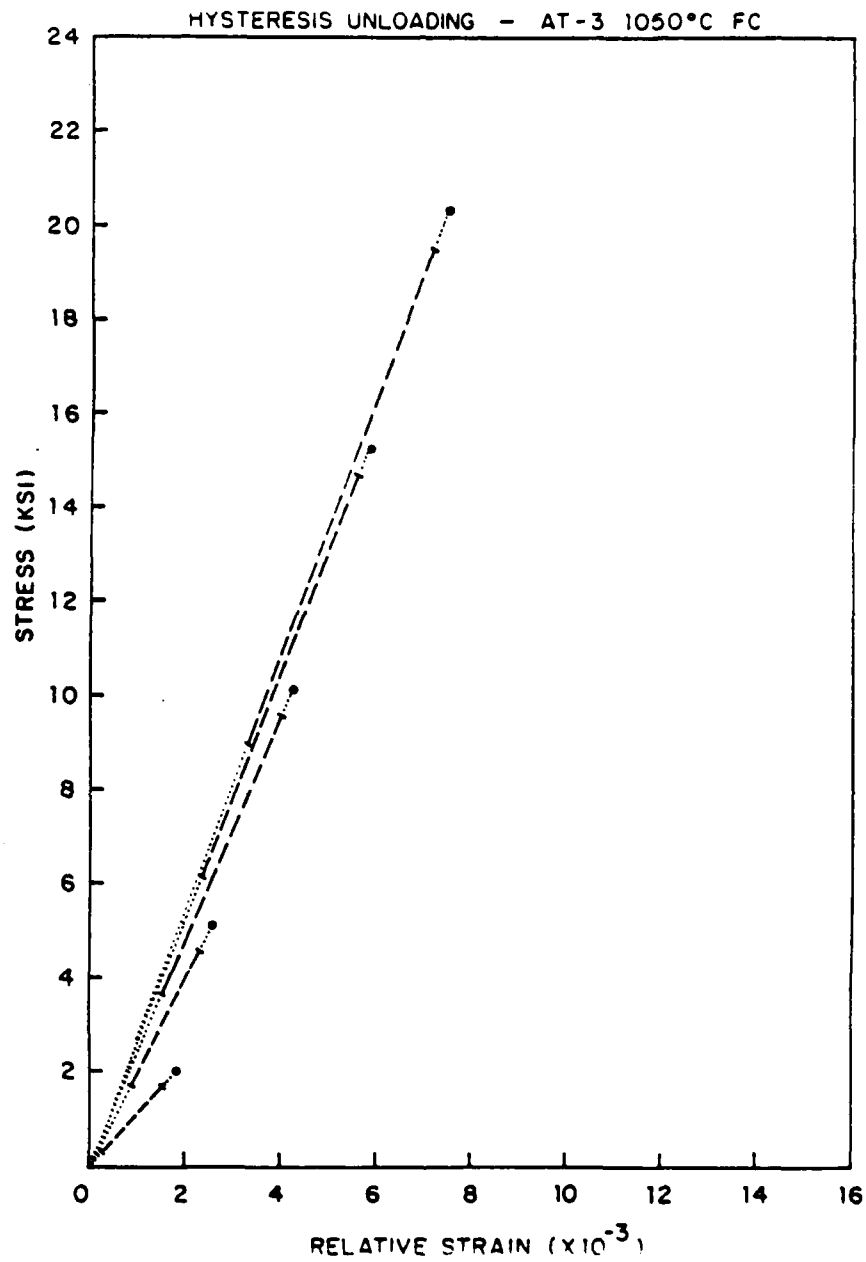Figure 3.19   Fe-Cr-Al 1050°C Tensile Hysteresis
Loading Slopes

52

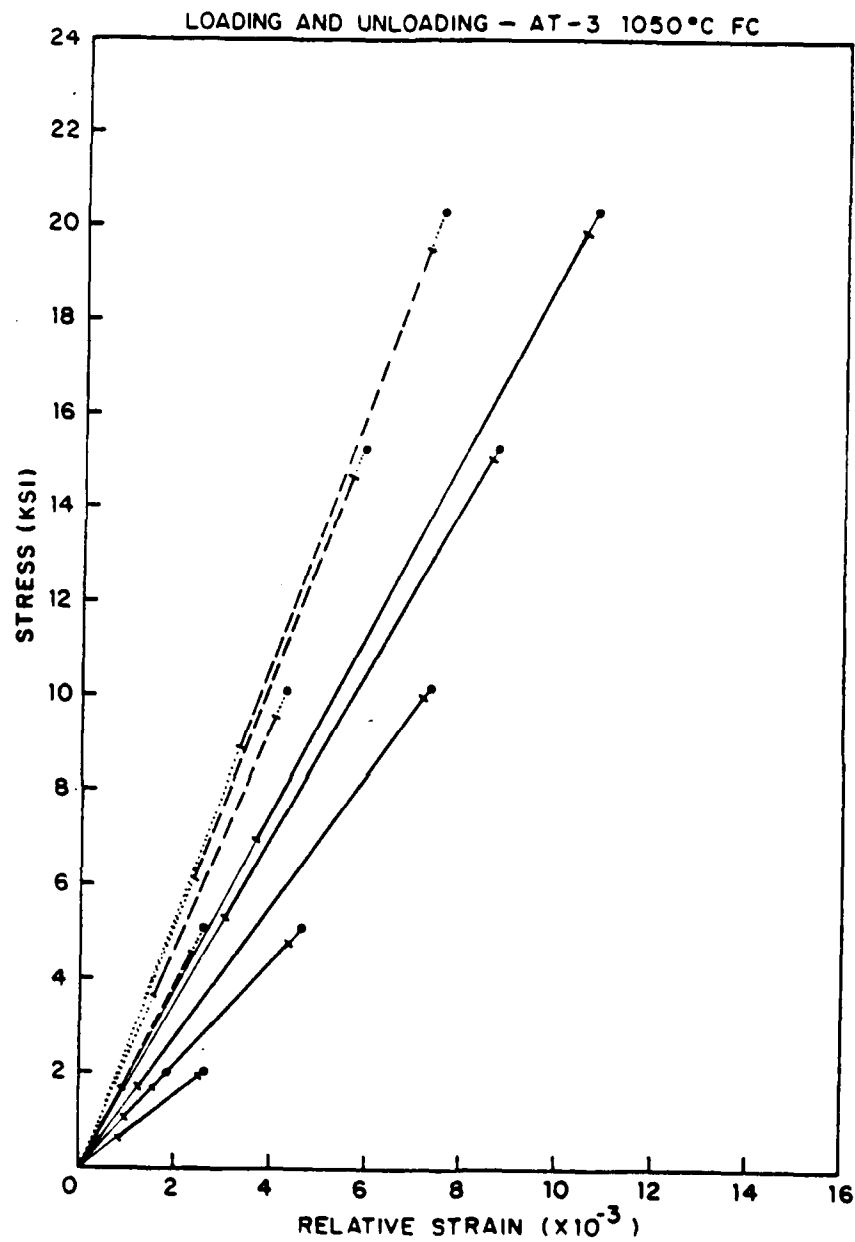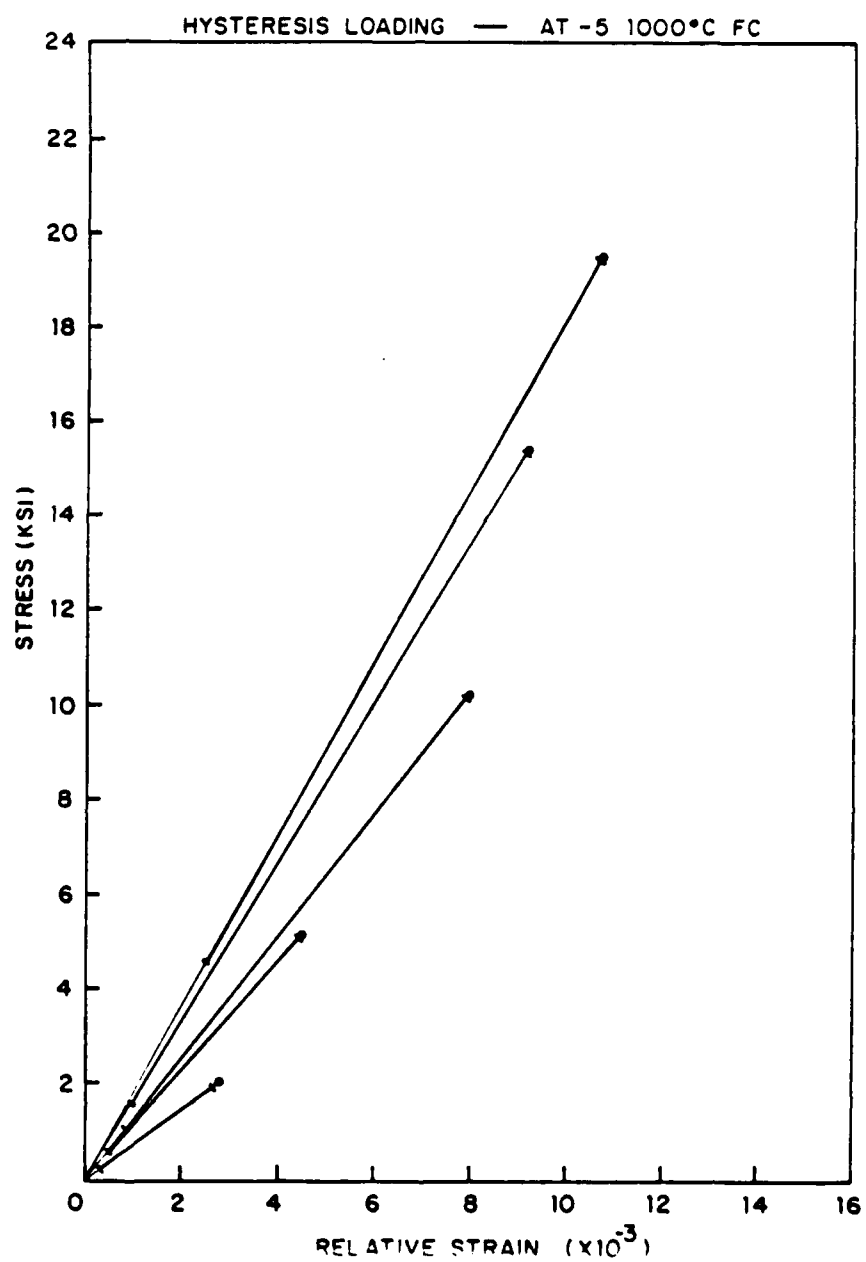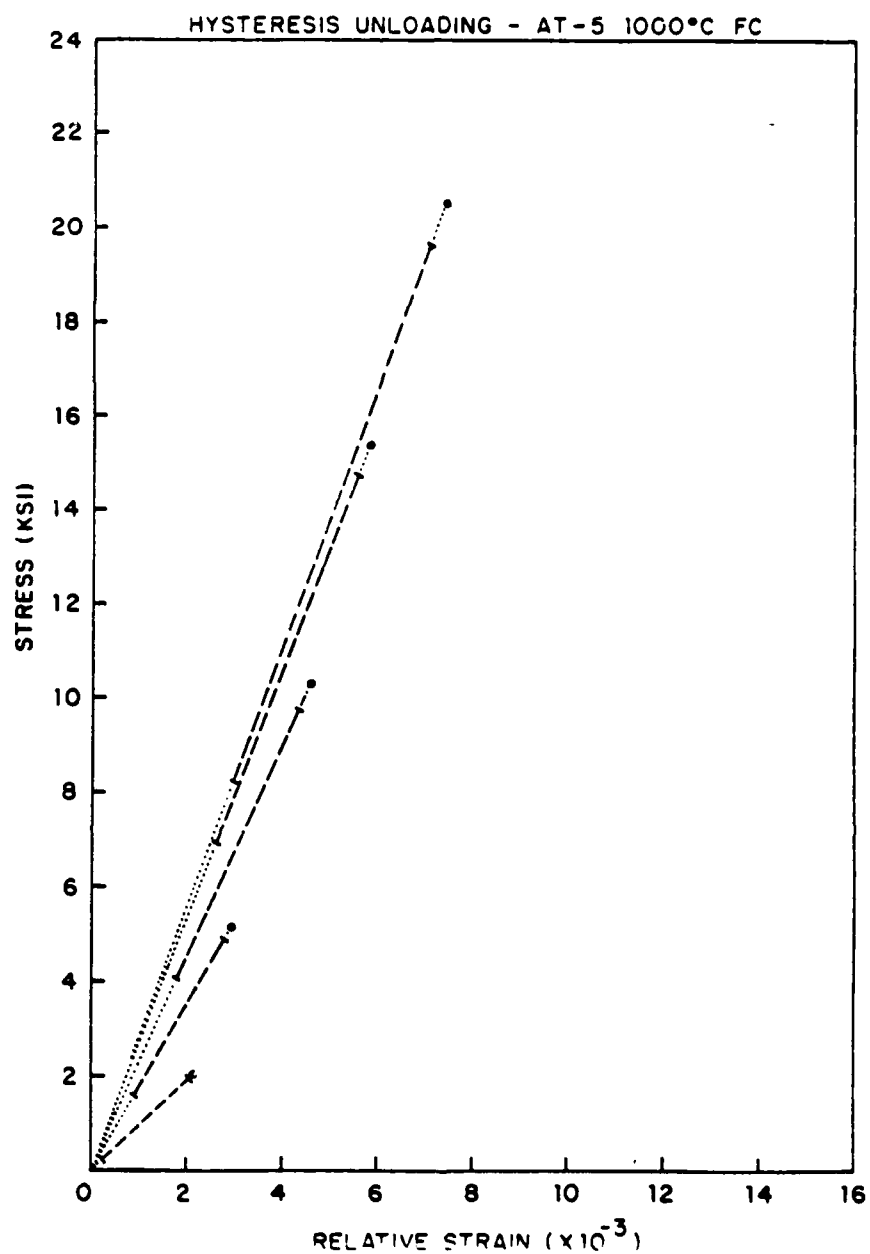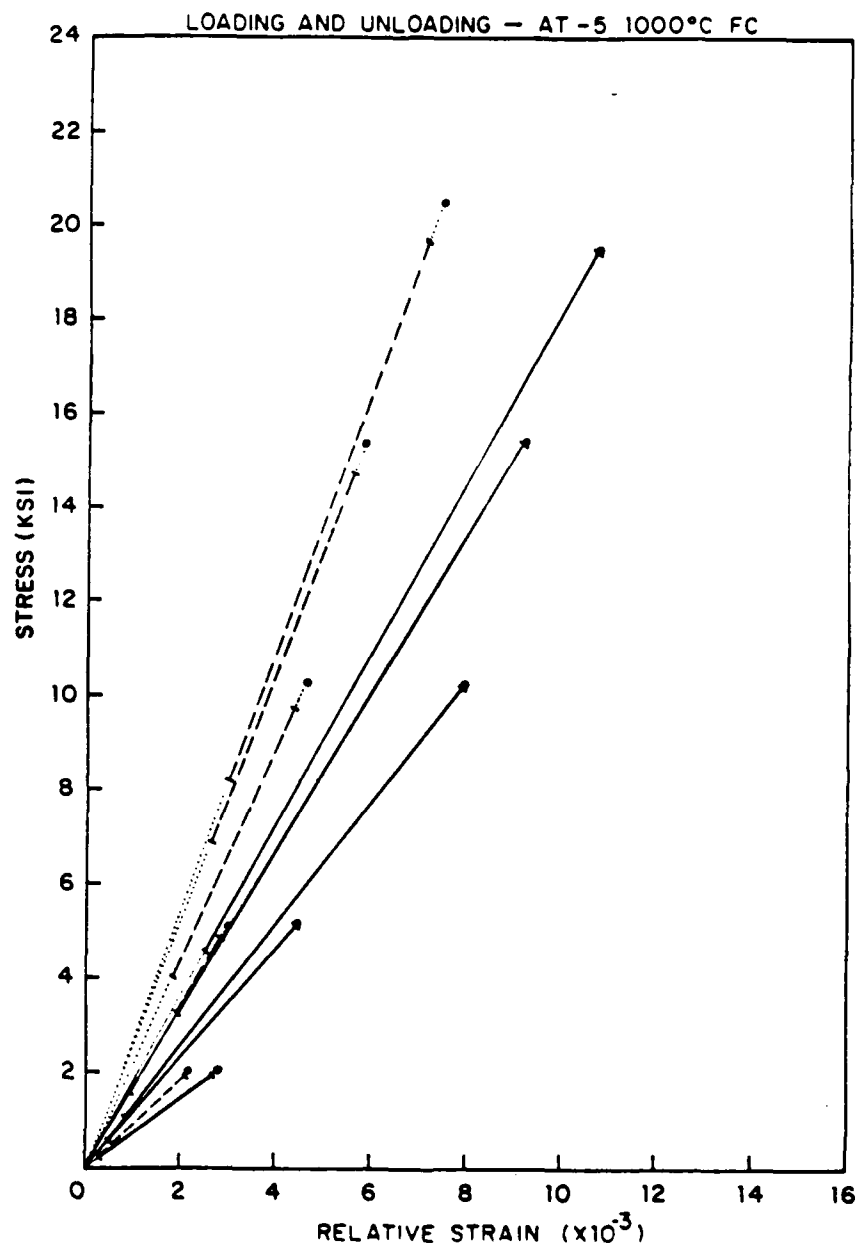Figure 3.20   Fe-Cr-Al 1050°C Tensile Hysteresis
Unloading Slopes

53

Figure 3.21   Fe-Cr-Al 1050°C Combined Tensile
Hysteresis Slopes

54

Figure 3.22   Fe-Cr-Al 1000°C Tensile Hysteresis
             Loading Slopes

55

Figure 3.23   Fe-Cr-Al 1000°C Tensile Hysteresis
Unloading Slopes

56

Figure 3.24   Fe-Cr-Al 1000°C Combined Tensile
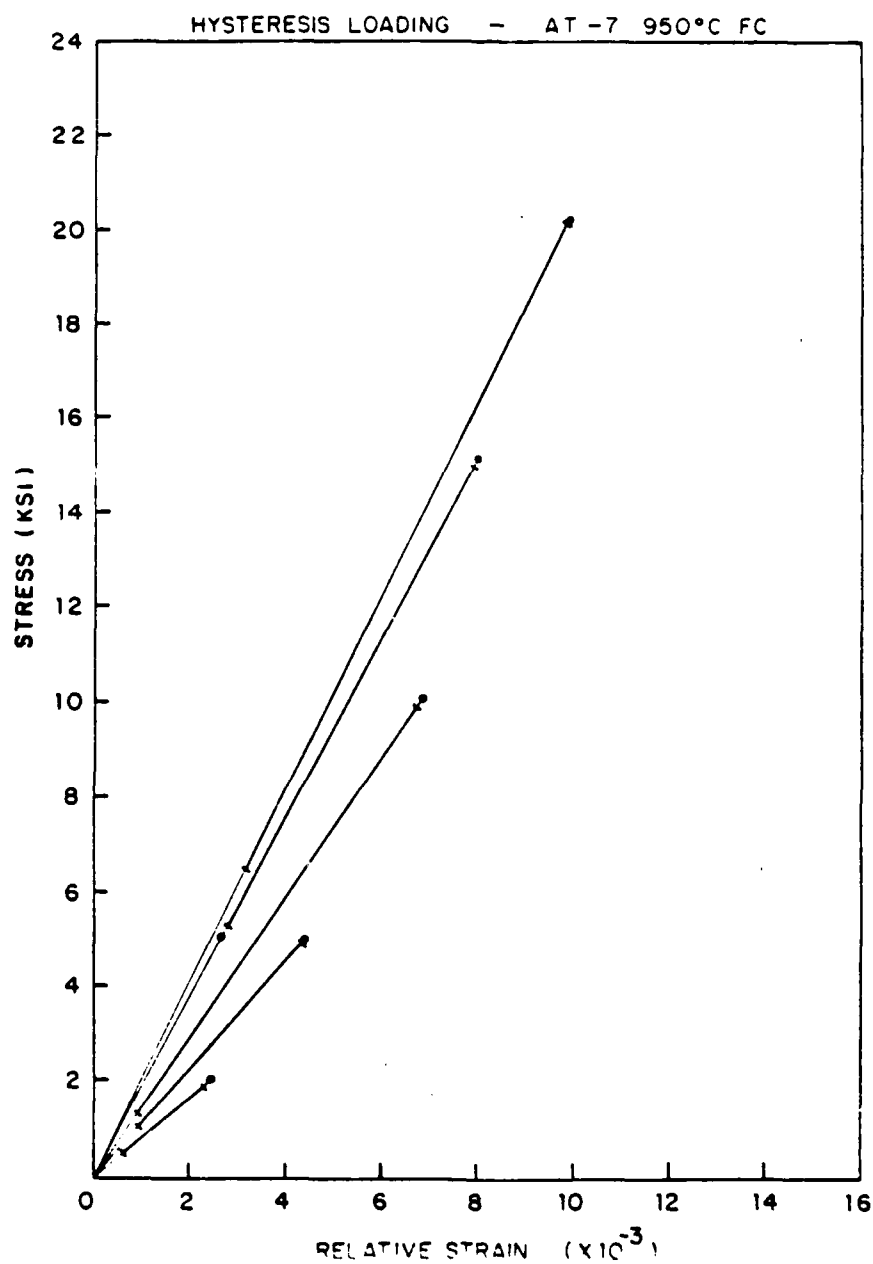Hysteresis Slopes

57

Figure 3.25   Fe-Cr-Al 950°C Tensile Hysteresis
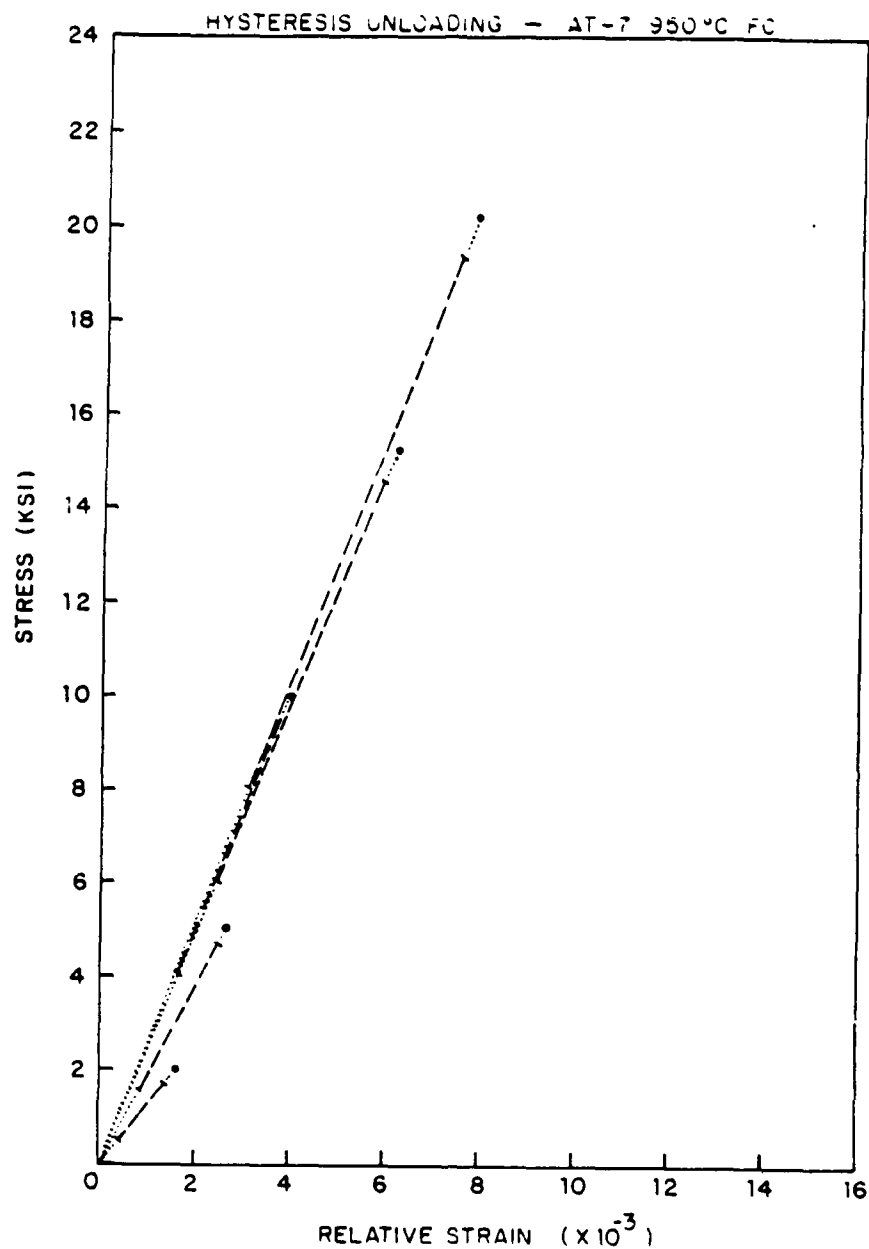Loading Slopes

58

Figure 3.26   Fe-Cr-Al 950°C Tensile Hysteresis
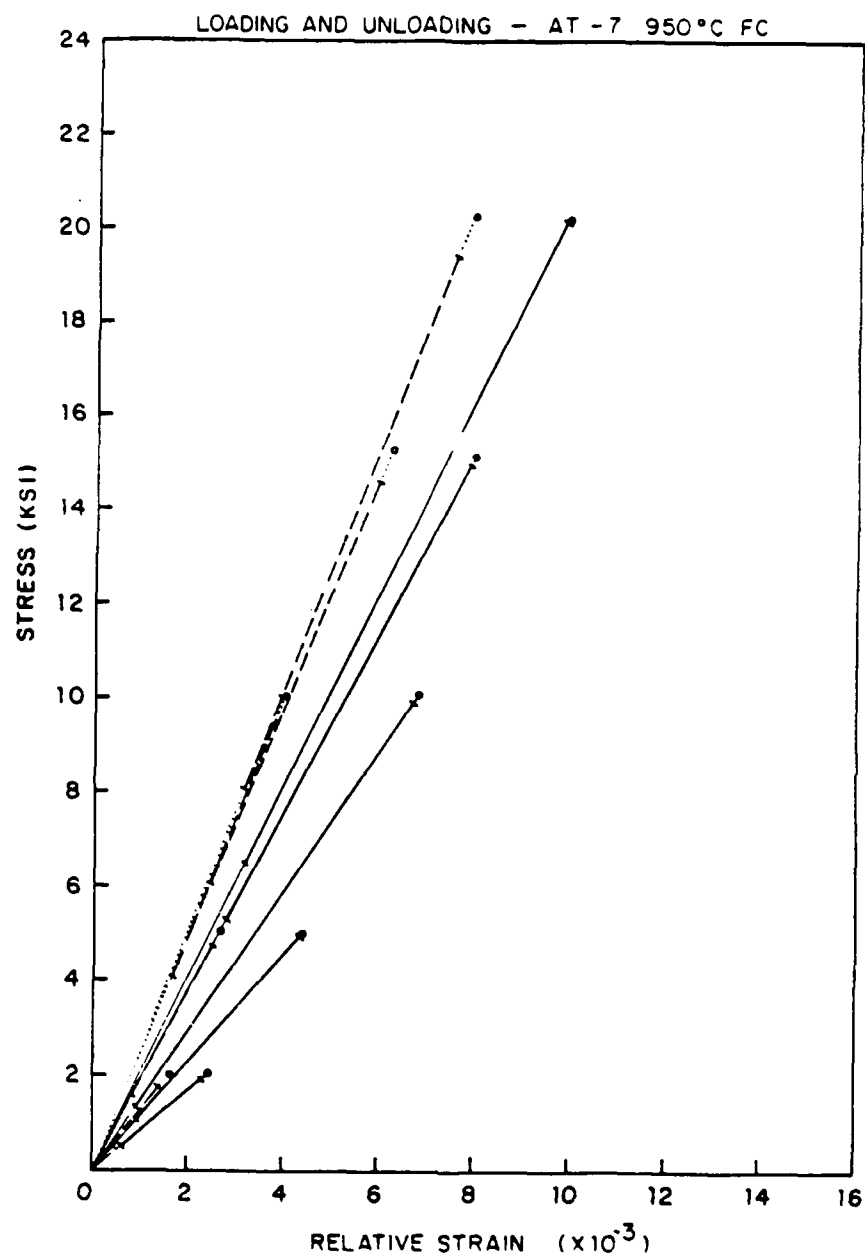Unloading Slopes

59

Figure 3.27   Fe-Cr-Al 950°C Combined Tensile
Hysteresis Slopes
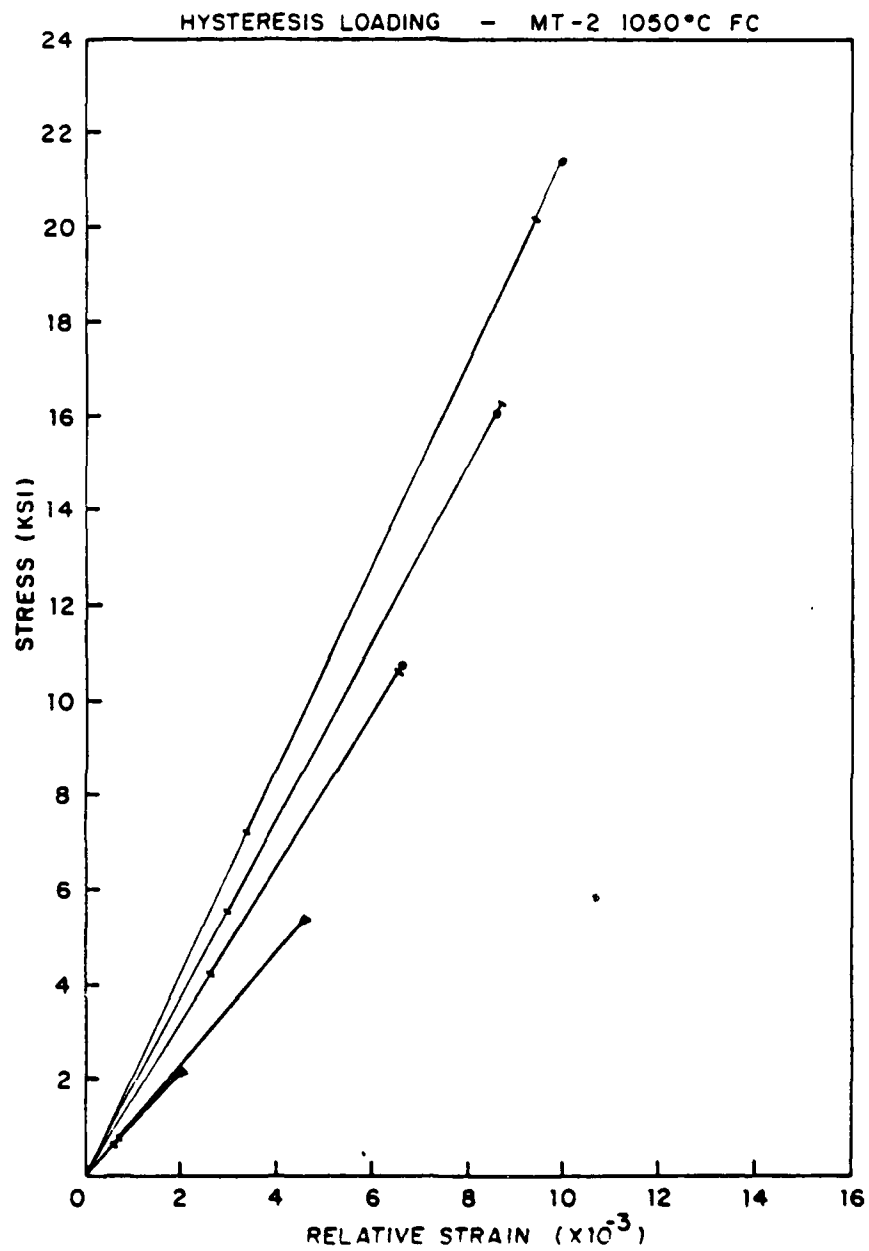
Figure 3.28   Fe-Cr-Mo 1050°C Tensile Hysteresis
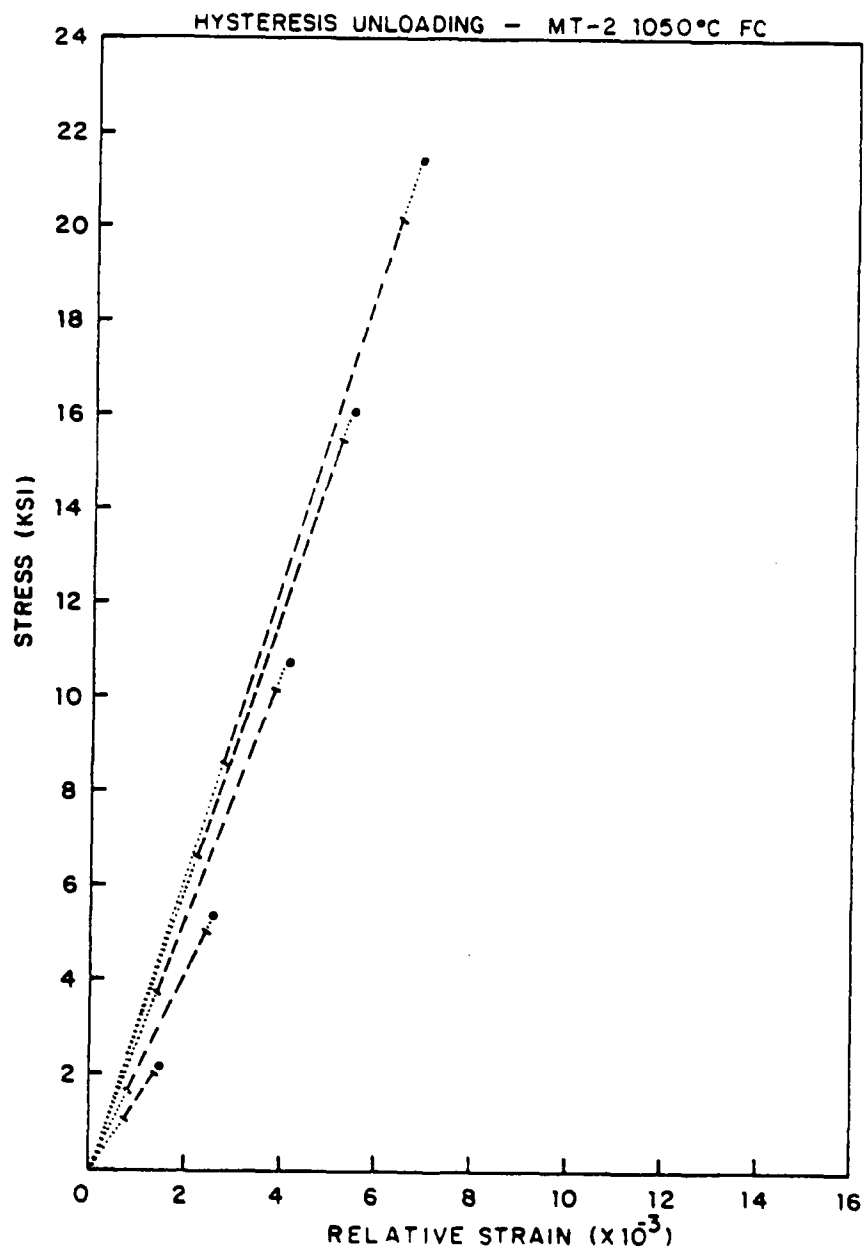   Loading Slopes

61

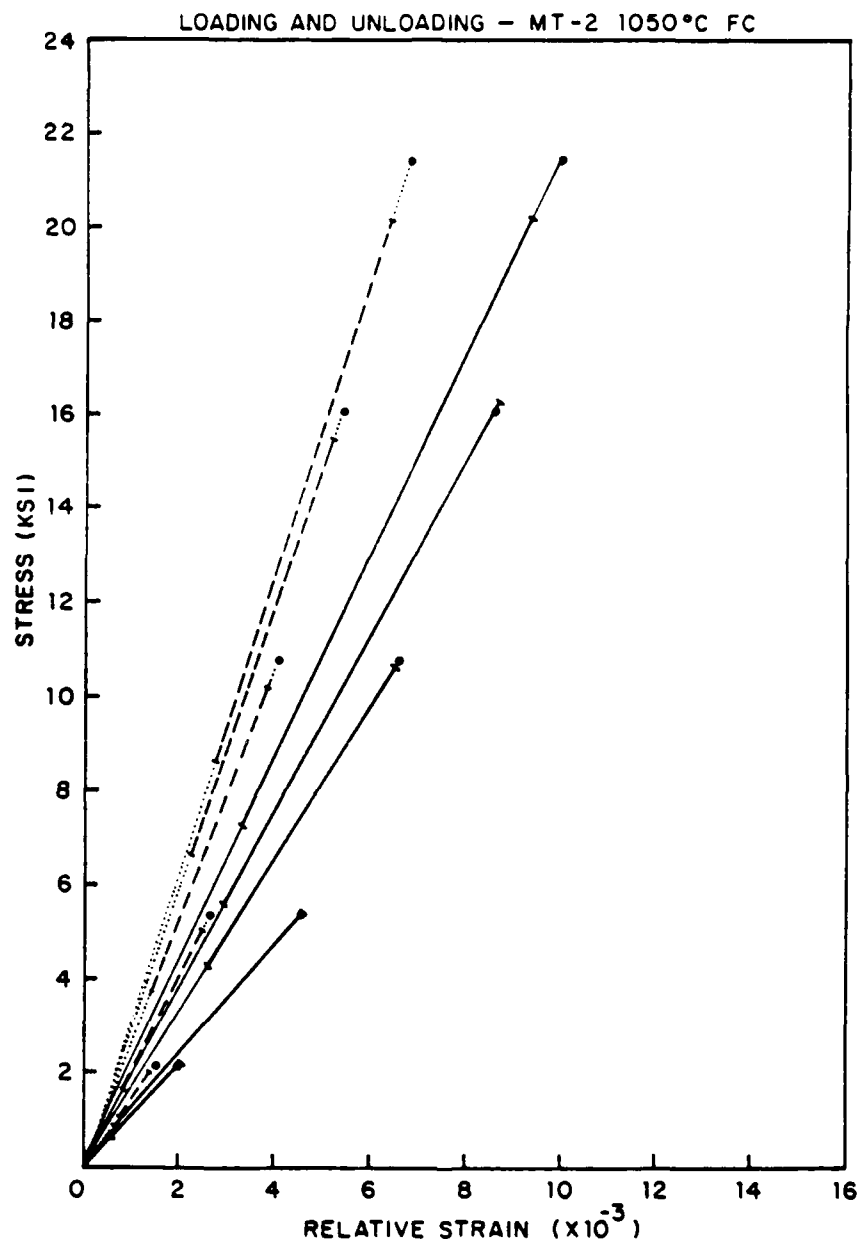Figure 3.29   Fe-Cr-Mo 1050°C Tensile Hysteresis
Unloading Slopes

Figure 3.30   Fe-Cr-Mo 1050°C Combined Tensile
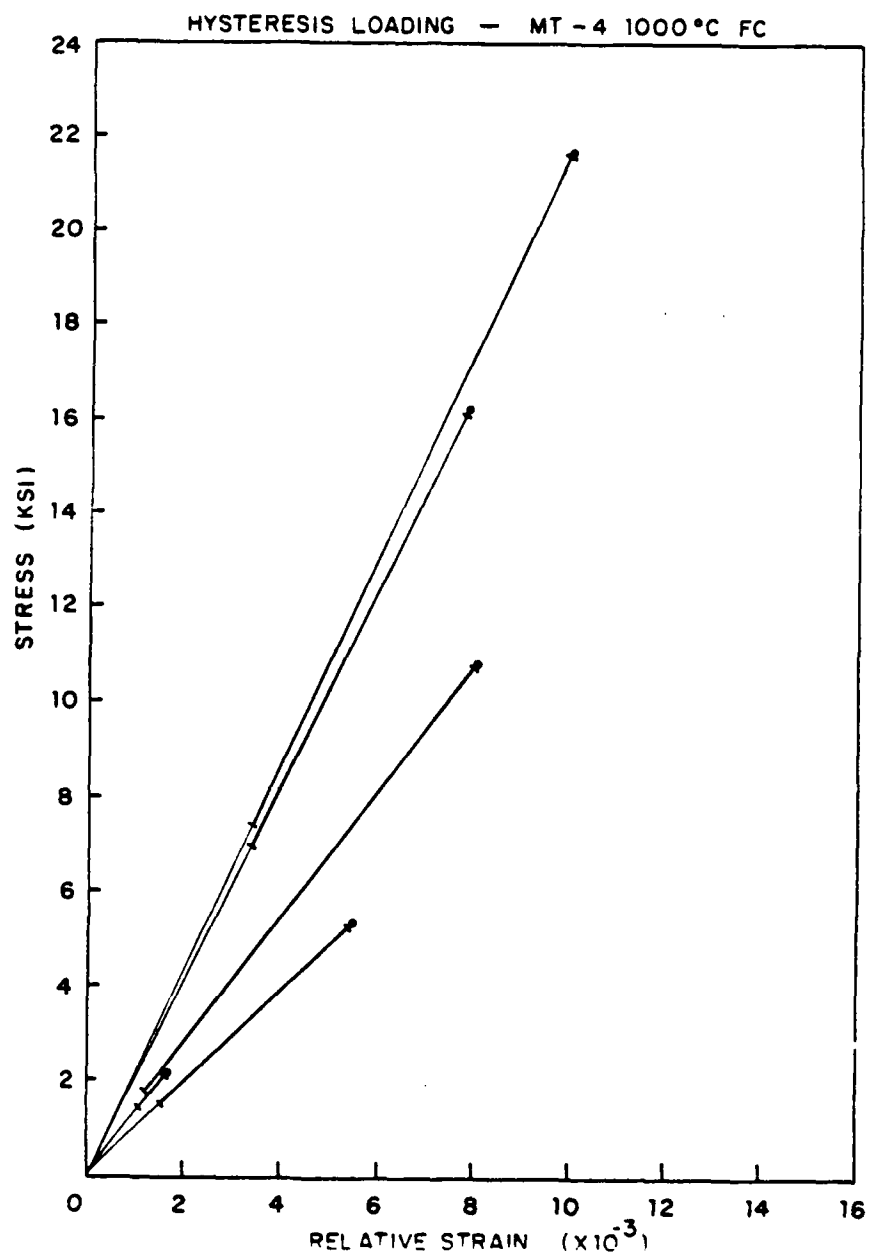Hysteresis Slopes

Figure 3.31   Fe-Cr-Mo 1000°C Tensile Hysteresis
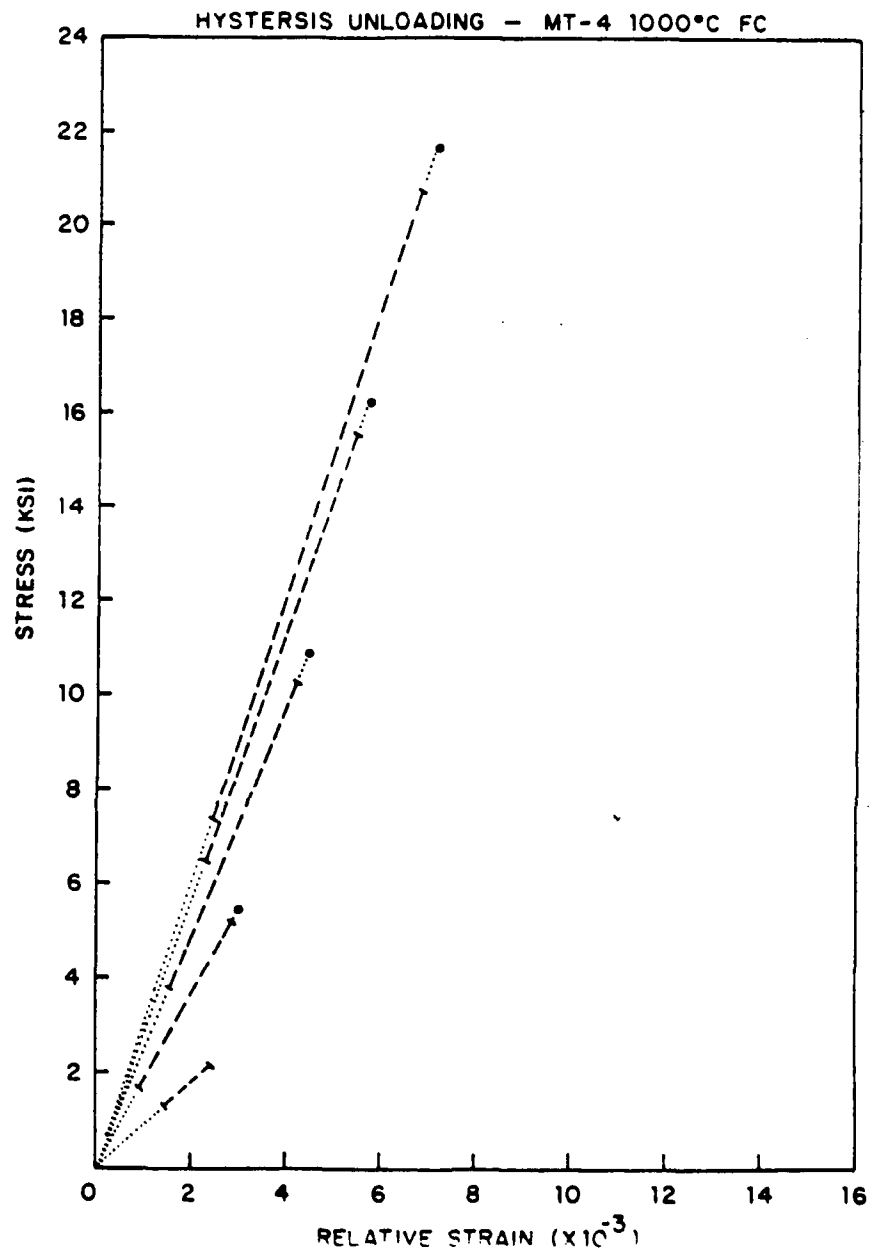Loading Slopes

64

Figure 3.32   Fe-Cr-Mo 1000°C Tensile Hysteresis
Unloading Slopes
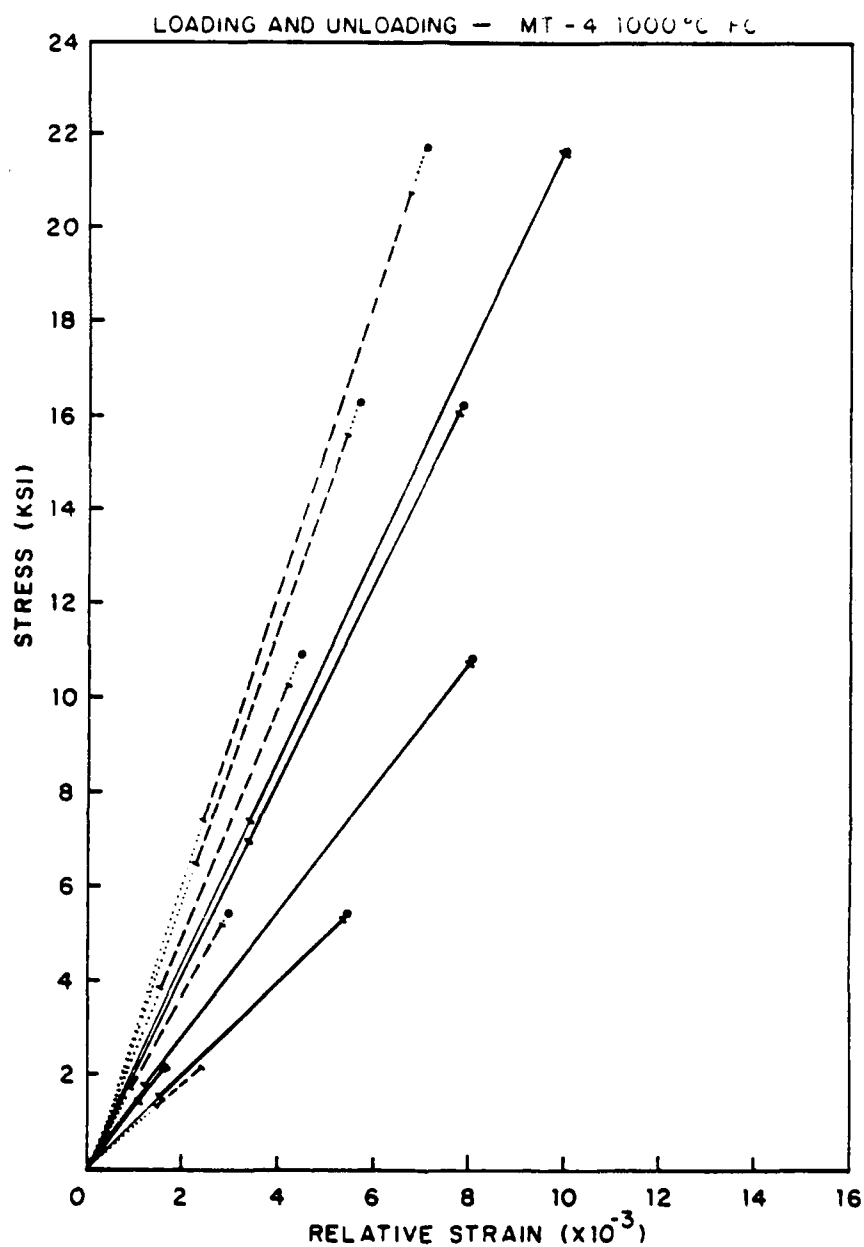
Figure 3.33   Fe-Cr-Mo 1000' C Combined Tensile
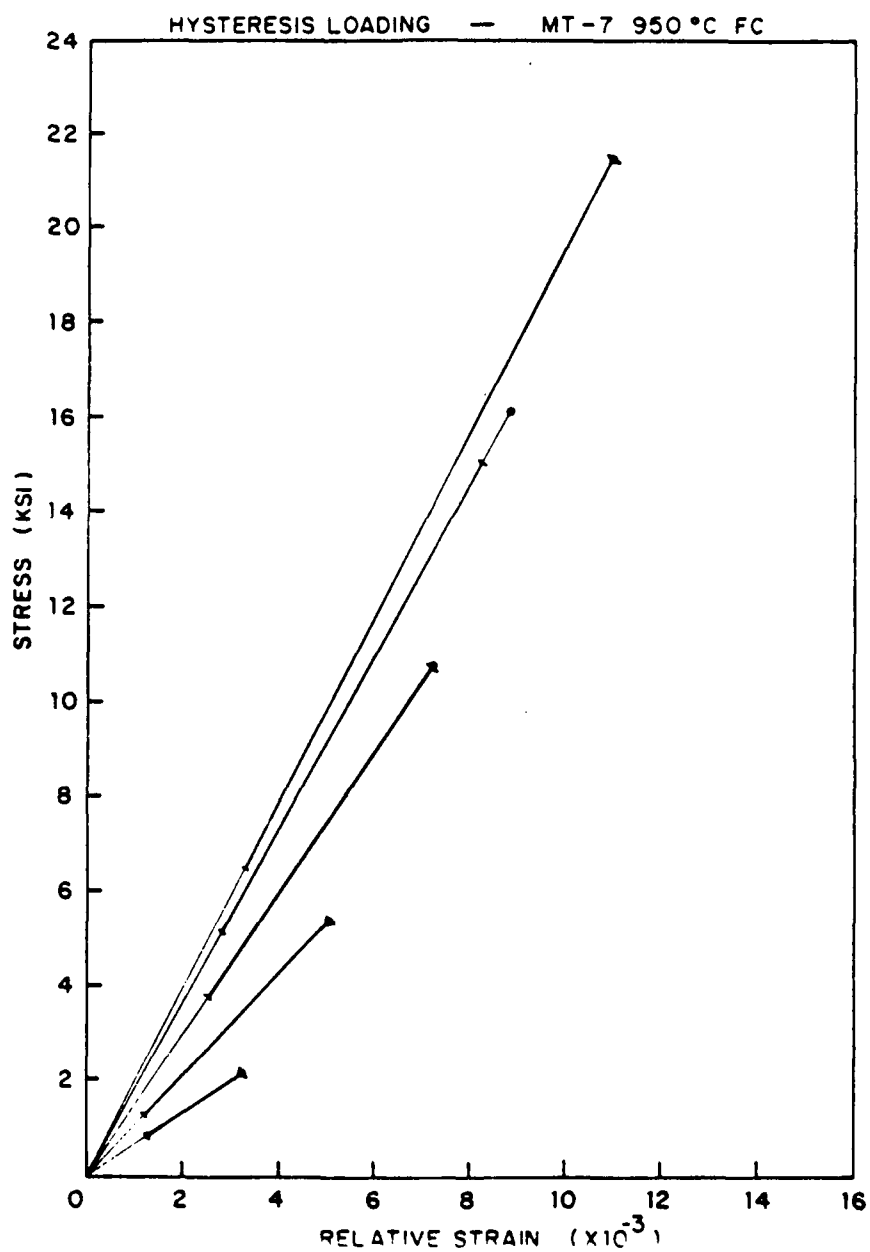   Hysteresis Slopes

66

Figure 3.34   Fe-Cr-Mo 950°C Tensile Hysteresis
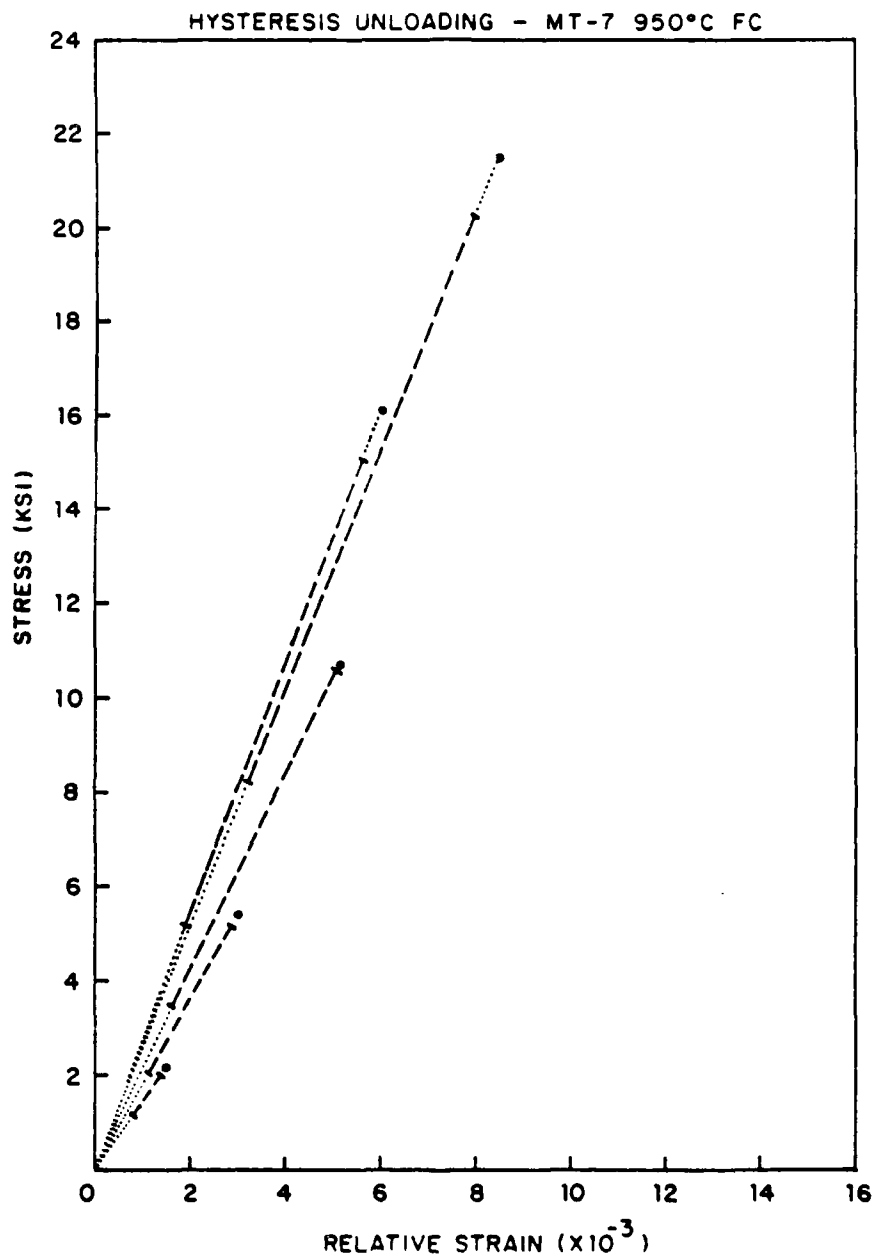   Loading Slopes

67

Figure 3.35   Fe-Cr-Mo 950°C Tensile Hysteresis
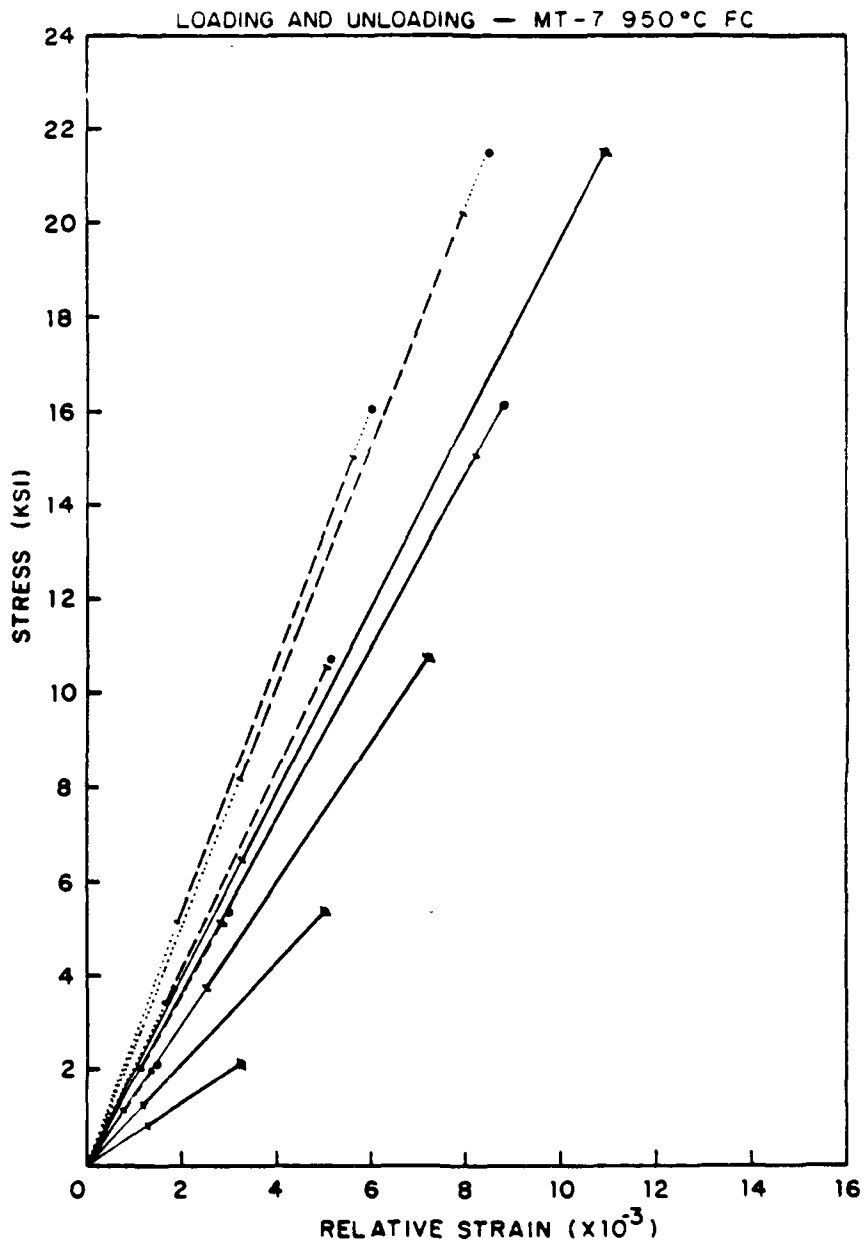Unloading Slopes

68

Figure 3.36   Fe-Cr-Mo 950°C Combined Tensile
Hysteresis Slopes

69

plots represent the actual section of the stress strain curve which coincides with this tangent line. The vertical axis is engineering stress (ksi) and the horizontal scale is relative strain (x 10^{-3}).

It is important to note that what is being presented in these figures is the slope of the upper portion of the stress-strain curve only. The presentation should not be taken to mean that all the curves originated from the (relative) zero strain point. In addition, as presented earlier, all the curves were actually quite nonlinear at low stresses; a feature which has been omitted in the present figures.

It is significant to note the continuously increasing slopes (moduli) of both the loading and unloading curves, as the material apparently becomes more resistant to strain with increasing stress levels. In addition, typically there was a very rounded shoulder at the top of the unloading curve; this is represented in the presentation of Figures 3.16 to 3.36 by the distance between the highest represented stress-strain point (circle) and the upper limit of the bold, bracketed section of the tangent curve (the upper bracket). For clarity, the slopes of the loading curves are presented as solid lines; slopes of the unloading curves are presented as dashed lines.
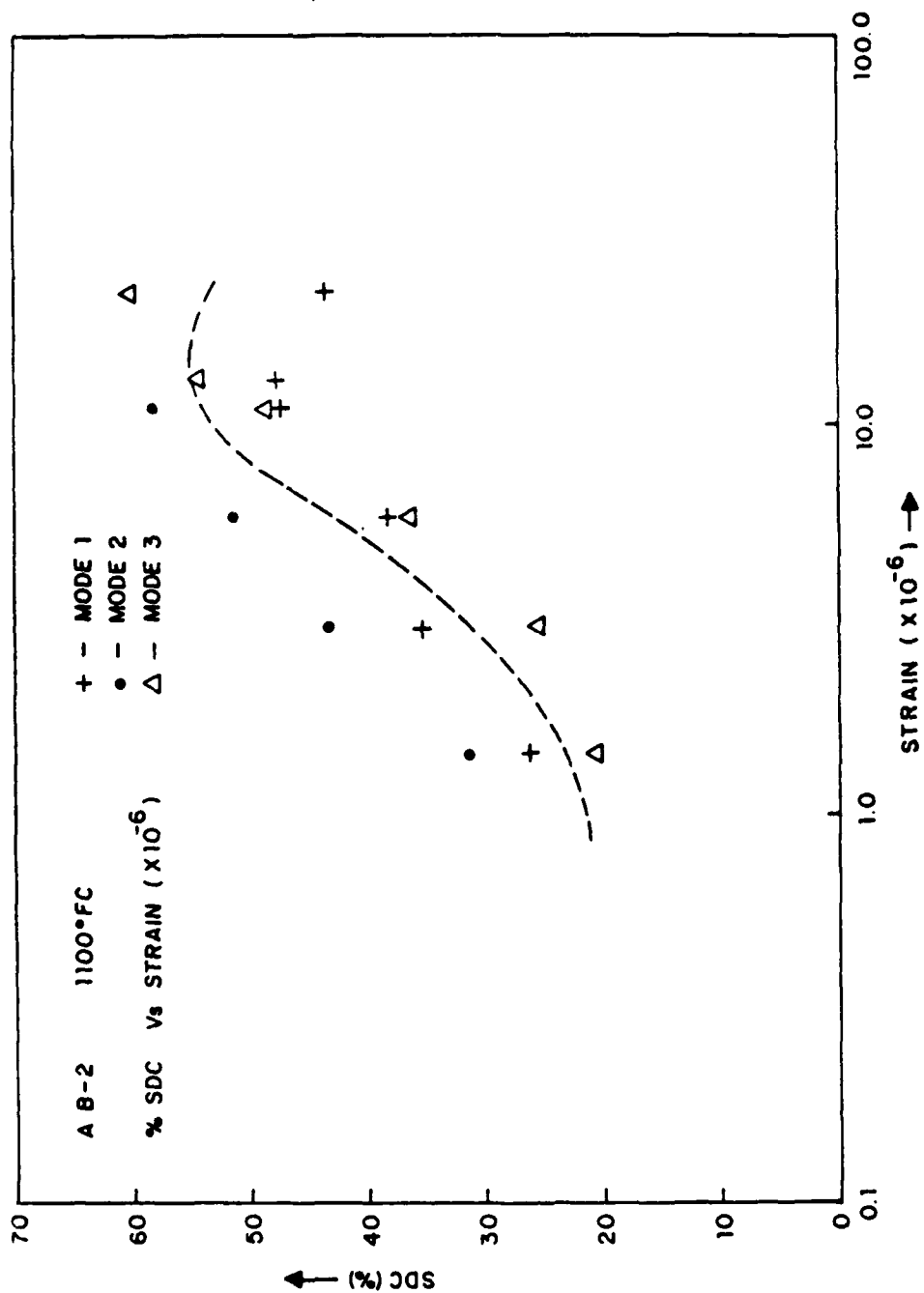
Figure 3.38 SDC vs. Strain for Fe-Cr-Al, 1100°C
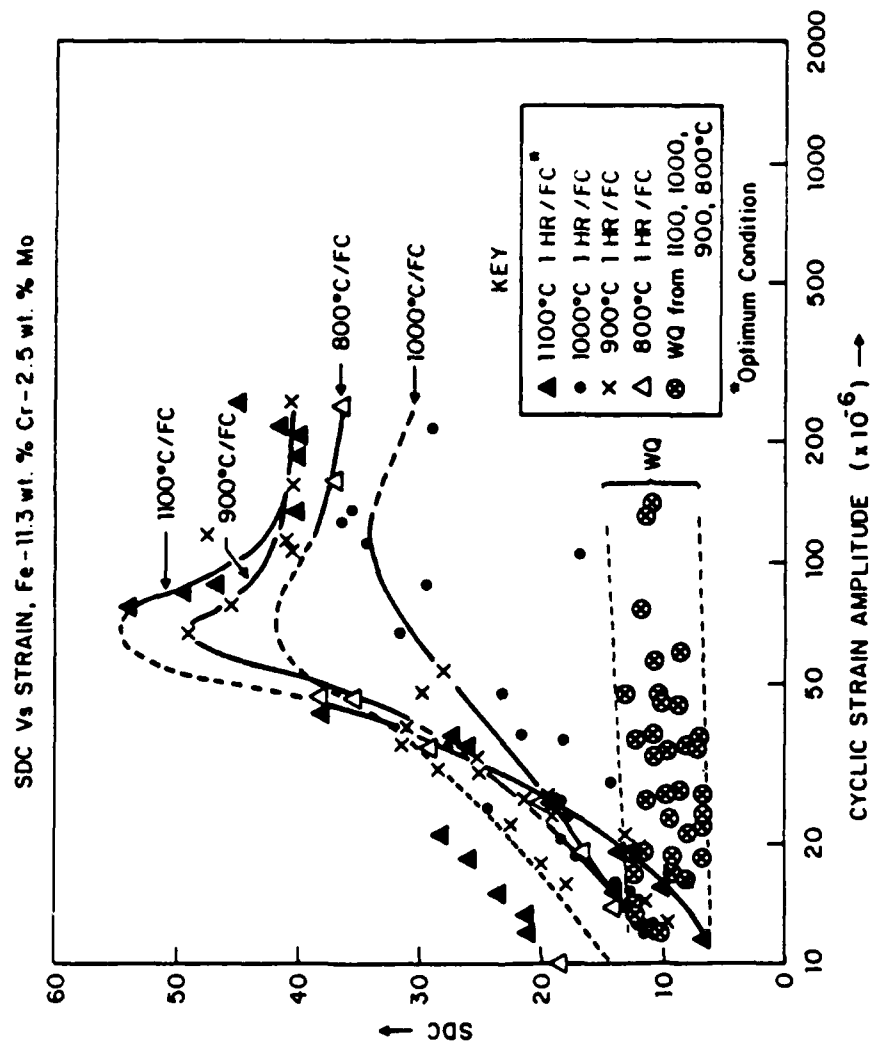Annealing Temperature, Furnace Cooled

74

Figure 3.37 SDC vs. Strain for an Fe-Cr-Mo Alloy as a Function of Heat Treatment

73

sample is displaced downward and to the right, corresponding to lower peak SDC, the peak occurring at a higher strain.

C. DAMPING CHARACTERISTICS

In his investigation of an Fe-Cr-Mo alloy, O'Toole [Ref. 6] reported a significant difference in the damping capacity of the 1000°C furnace cooled sample as compared to the other furnace cooled specimens (see Figure 3.37). Specifically, the 1000° sample required higher strain to activate the damping mechanism and the maximum specific damping capacity was significantly less.

To relate this to results of the present investigations, Figures 3.38 to 3.41 present the relationship of specific damping capacity (SDC) to average peak strain for the Fe-Cr-Al alloy, and Figure 3.42 is a composite of these. These results indicate no significant difference due to heat treatment temperature for furnace cooled Fe-Cr-Al alloy specimens. In fact, the 1000° curve is slightly displaced to the lower strains, an effect opposite to that reported by O'Toole for an Fe-Cr-Mo alloy at 1000°C heat treatment. In addition, the peak SDC is approximately the same as the other samples.

Results from the Fe-Cr-Mo alloy investigated here (which was not exactly the same ingot material as used by O'Toole) are presented in Figures 3.43 to 3.45, showing the relationship of SDC to average peak strain. These curves are combined in Figure 3.46. Consistent with O'Toole's results, the data for the alloy when heat treated at 1000°C

71

Figure 3.39 SDC vs. Strain for Fe-Cr-Al, 1050°C
Annealing Temperature, Furnace Cooled

Figure 3.40 SDC vs. Strain for Fe-Cr-Al, 1000°C Annealing Temperature, Furnace Cooled

Figure 3.41 SDC vs. Strain for Fe-Cr-Al, 950°C
Annealing Temperature, Furnace Cooled

Figure 3.42   SDC vs. Strain for Fe-Cr-Al as a Function of Heat Treatment Temperature
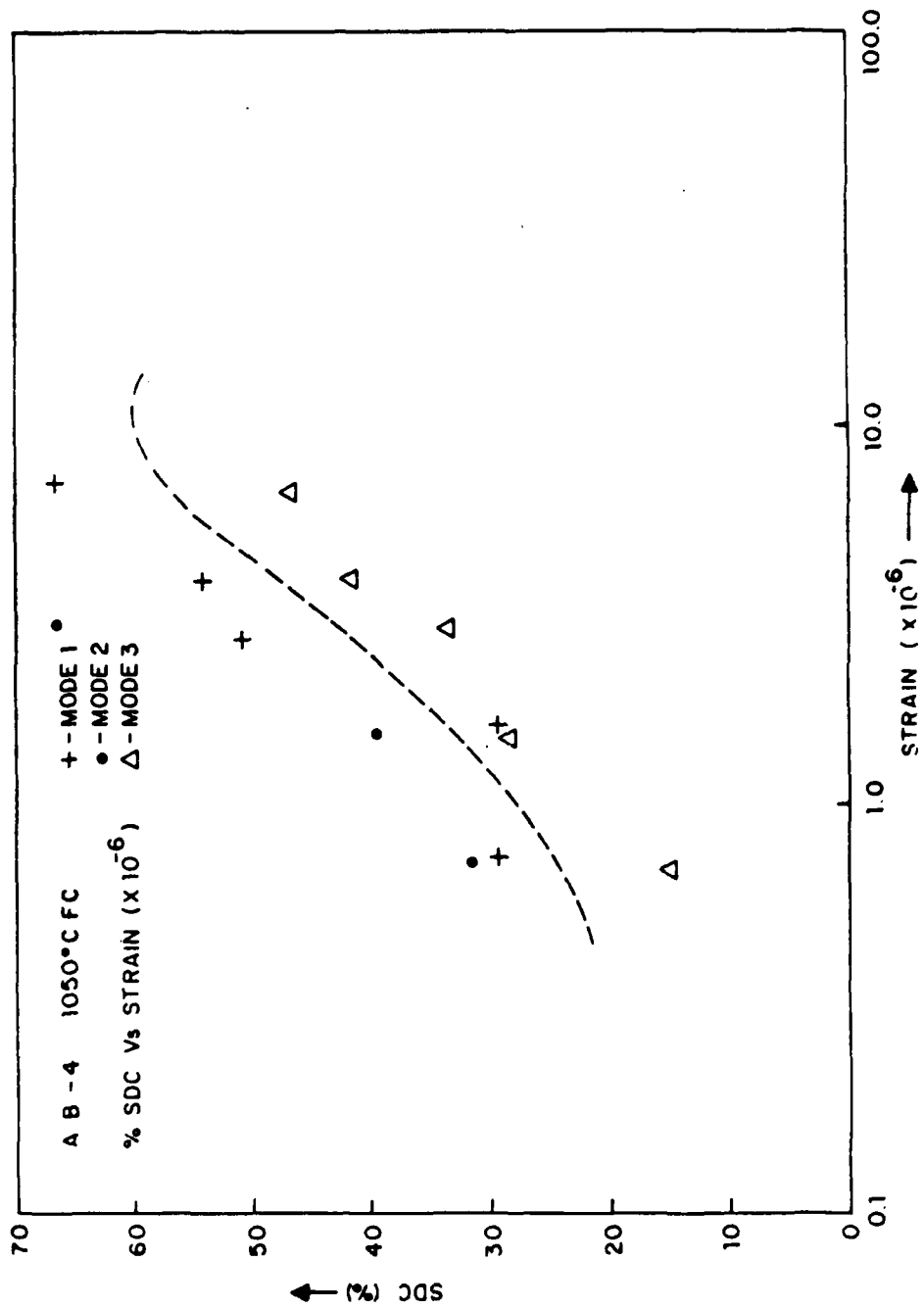
Figure 3.43 SDC vs. Strain for Fe-Cr-Mo, 1050°C Annealing Temperature, Furnace Cooled
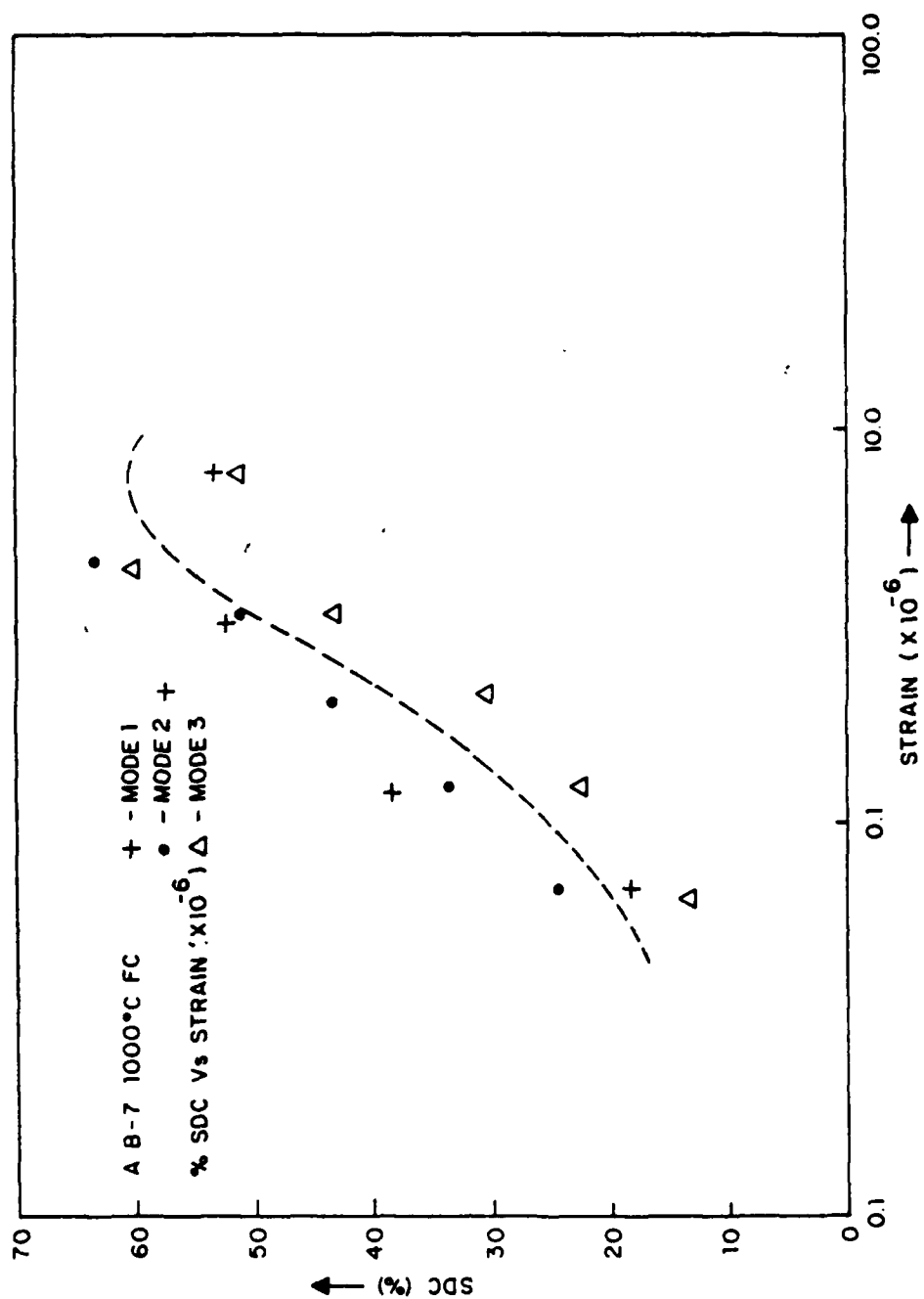
Figure 3.44 SDC vs. Strain for Fe-Cr-Mo, 1000°C
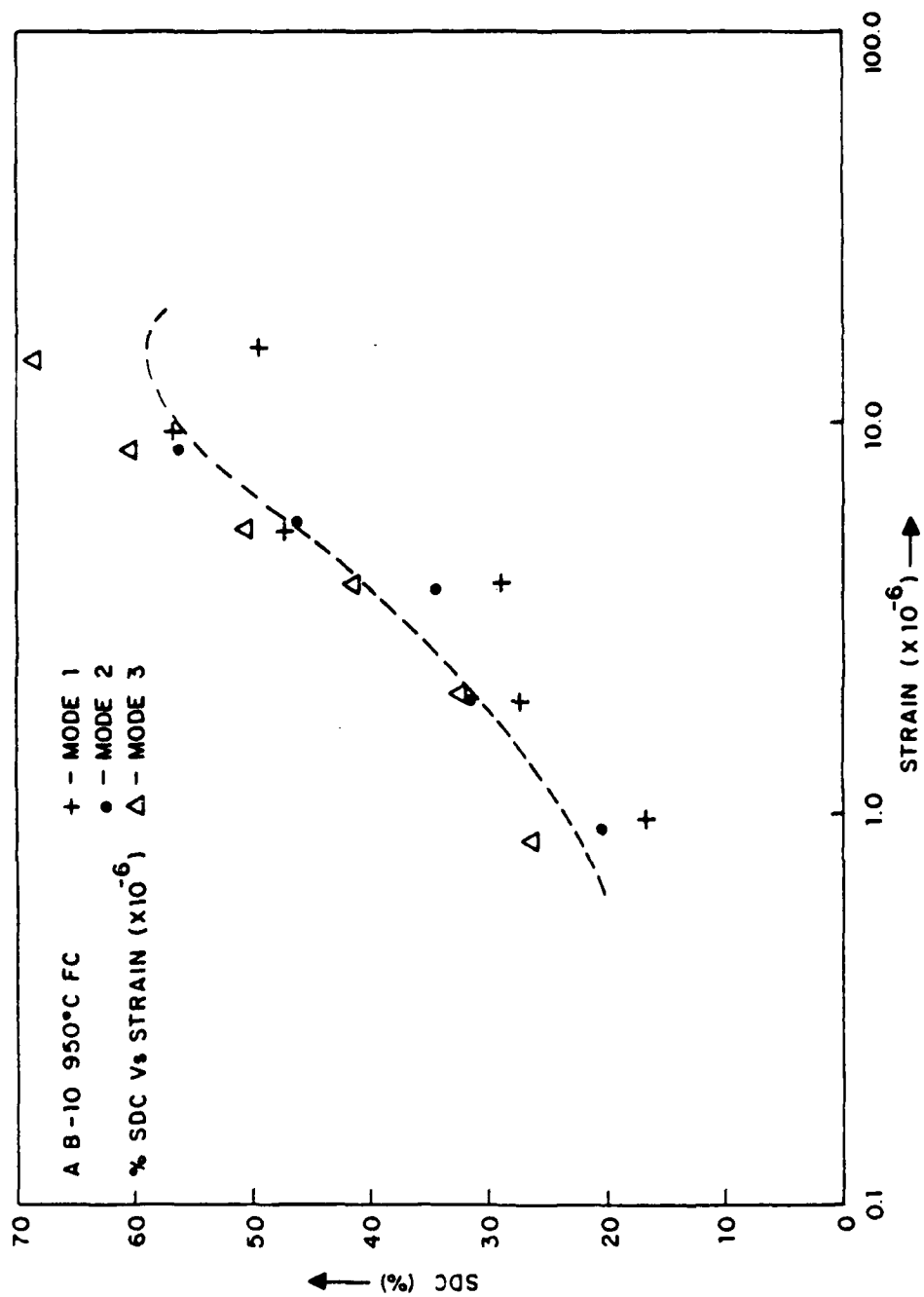Annealing Temperature, Furnace Cooled

Figure 3.45 SDC vs. Strain for Fe-Cr-Mo, 950°C
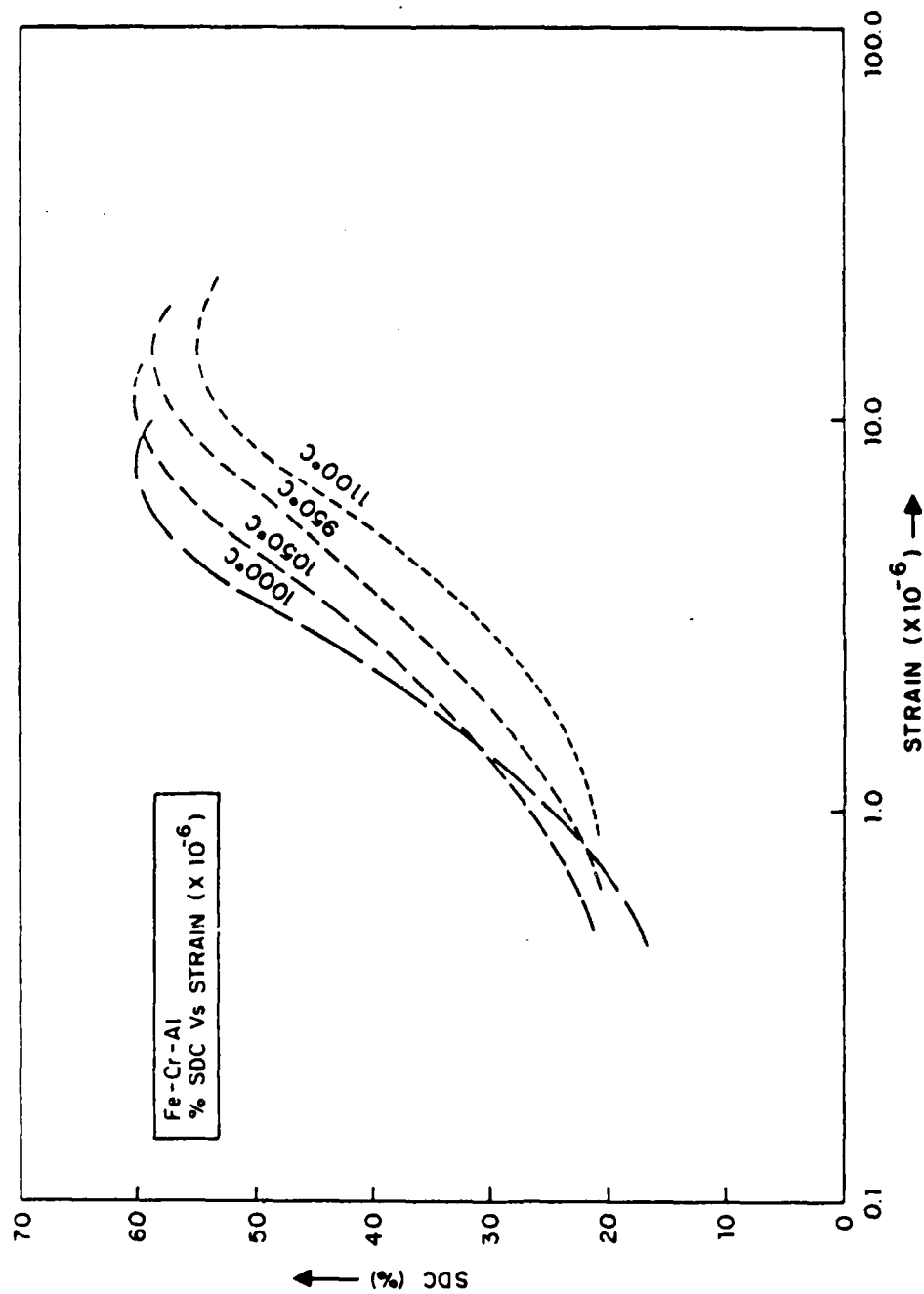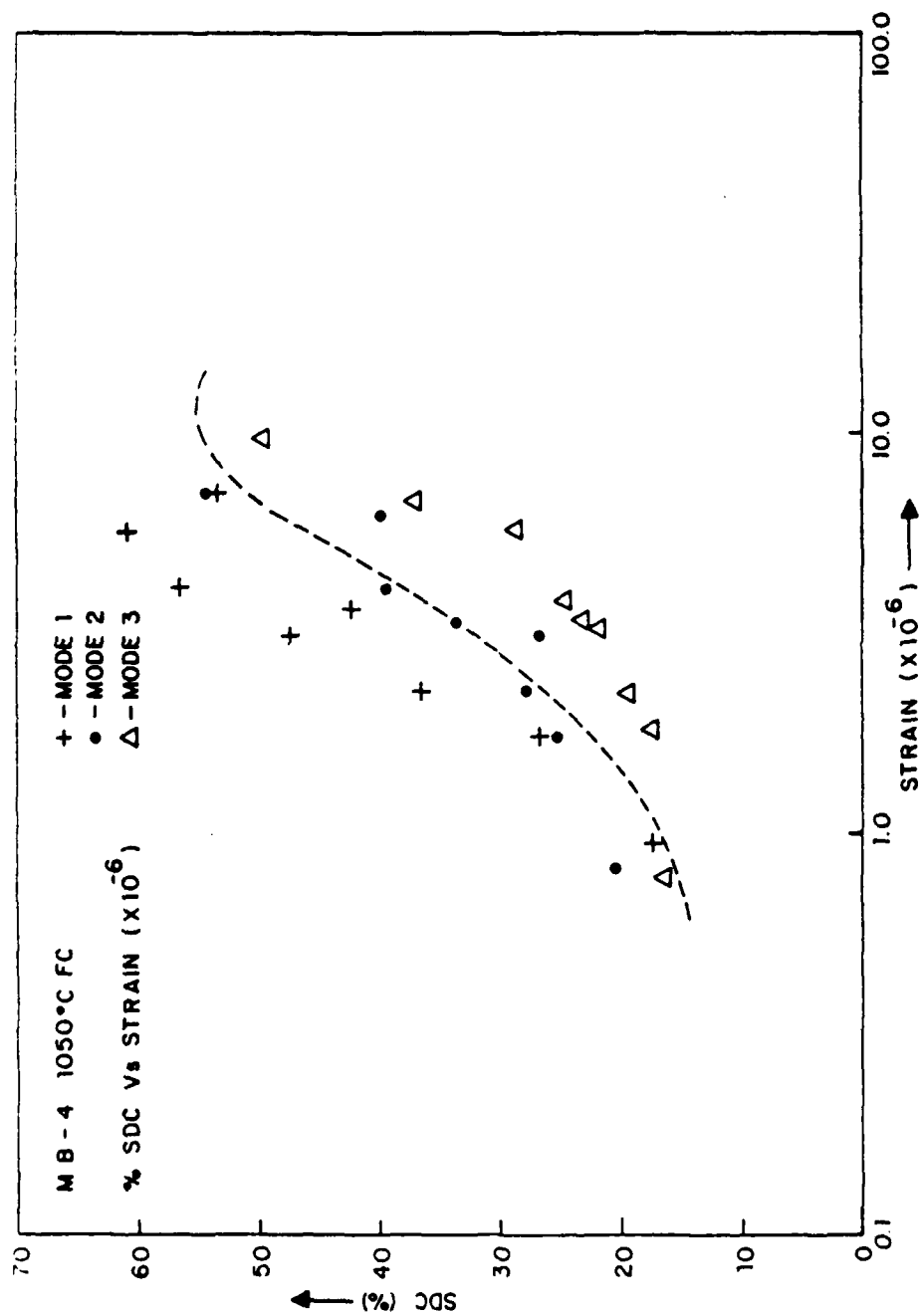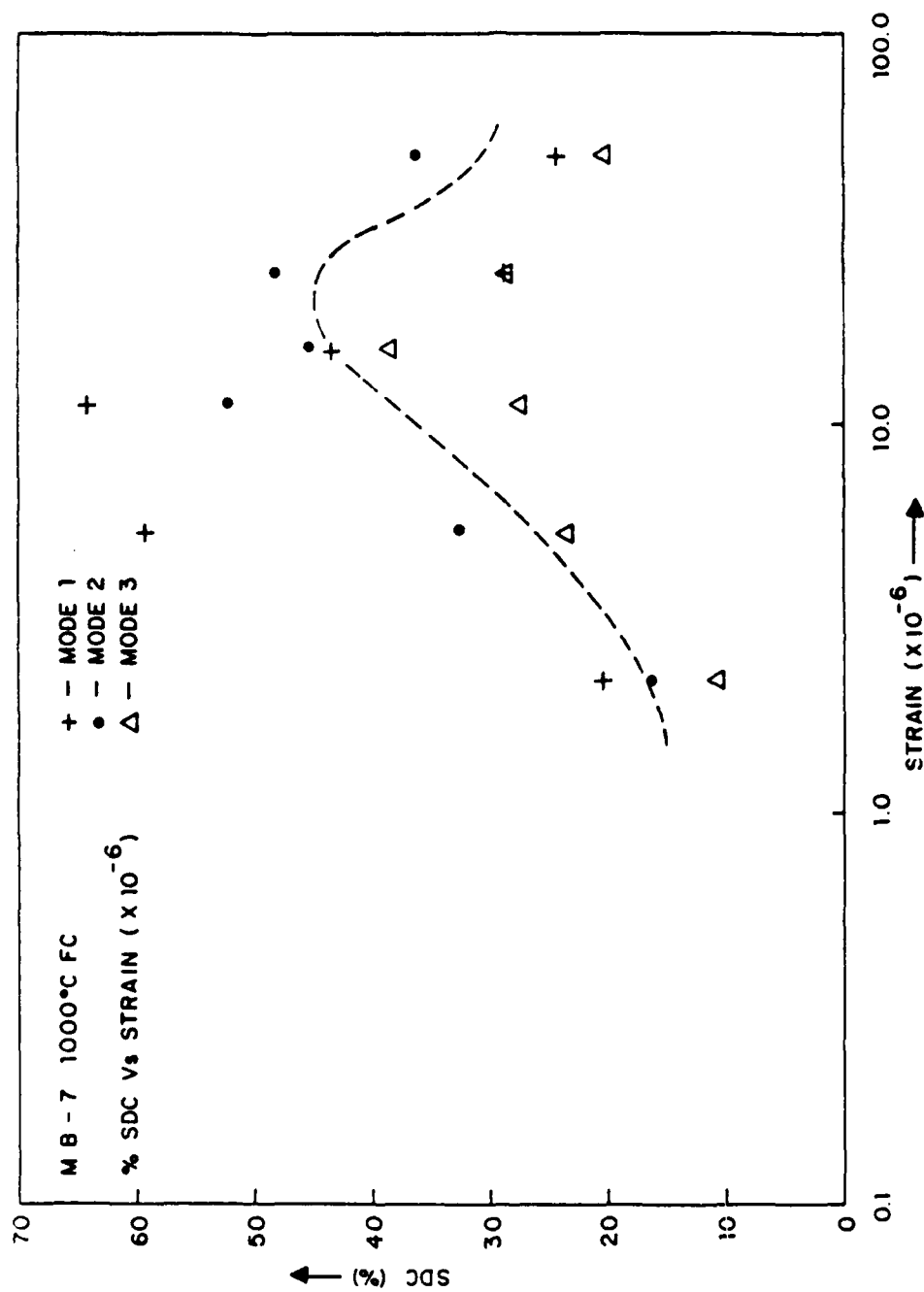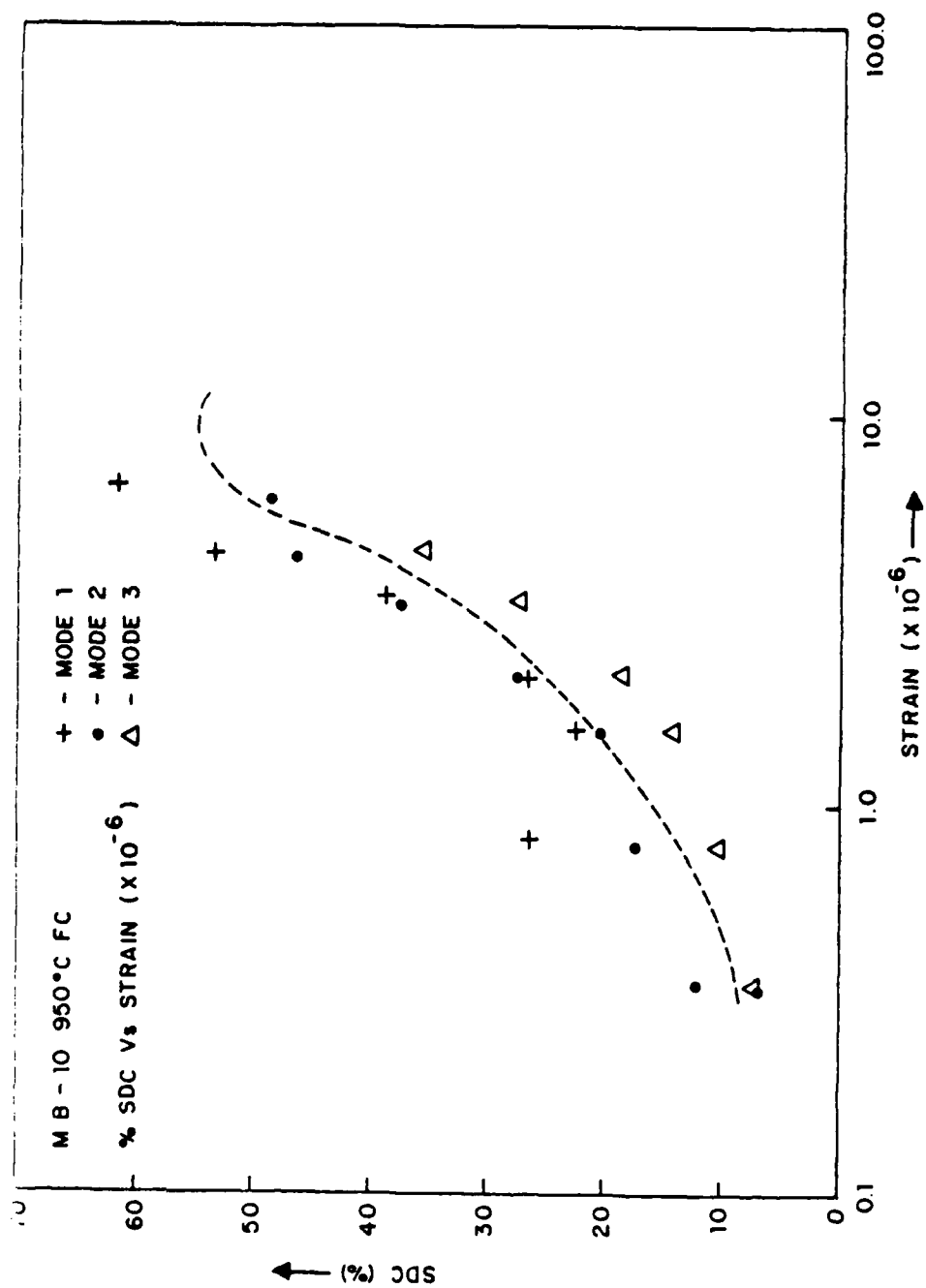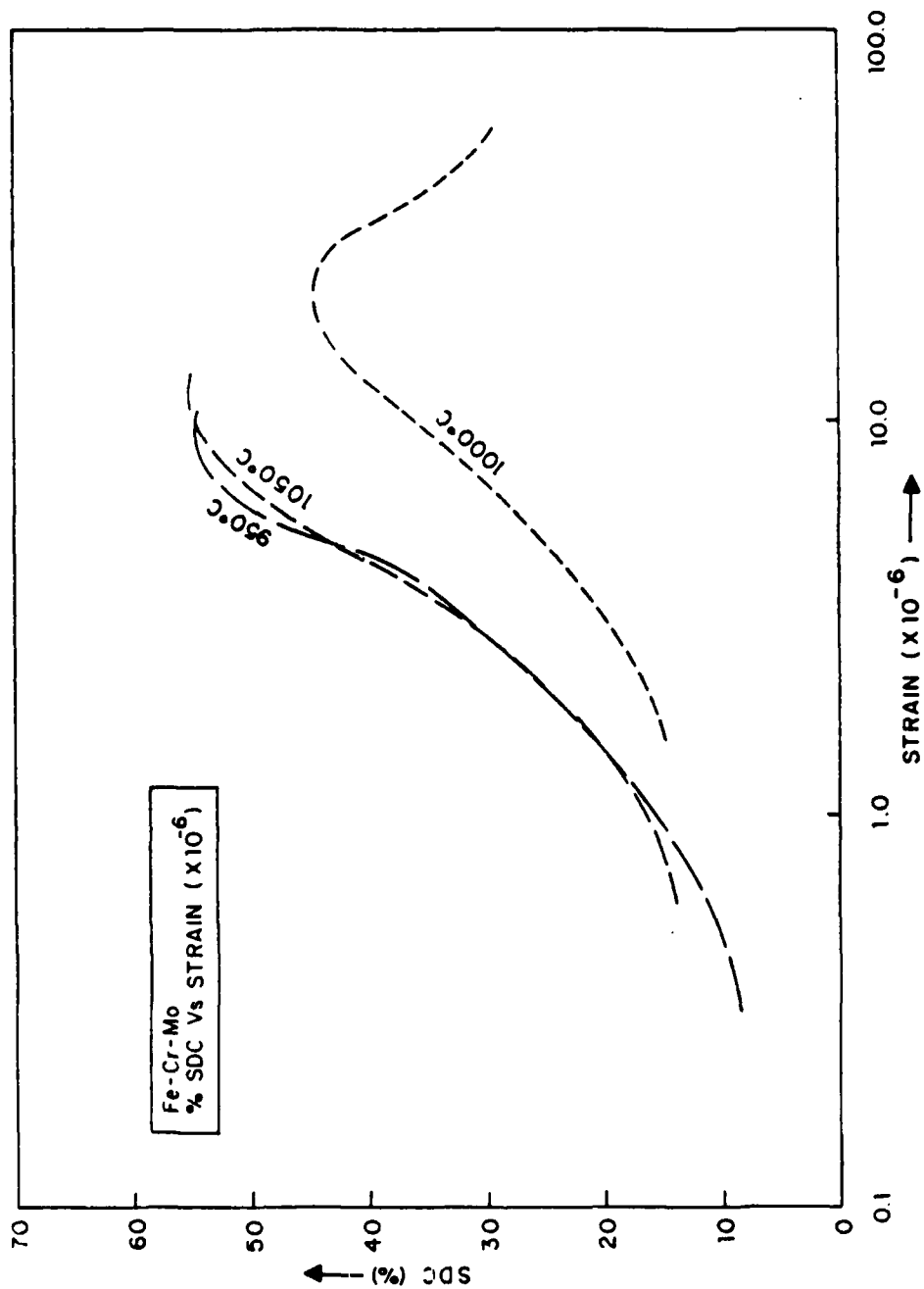Annealing Temperature, Furnace Cooled

81

Figure 3.46 SDC vs. Strain for Fe-Cr-Mo as a Function of Heat Treatment Temperature

82

IV. CONCLUSIONS AND RECOMMENDATIONS

A. CONCLUSIONS

1. A phase change in the furnace cooled Fe-Cr-Mo alloy was not detected by dilatometric measurements.

2. It has been demonstrated that a pseudoelastic effect is present for all furnace cooled tensile samples. This effect was more pronounced for the Fe-Cr-Mo alloy than for the Fe-Cr-Al alloy.

3. During tensile hysteresis testing, increasing strain levels produced a corresponding increase in the apparent elastic modulus of the sample.

4. Both Fe-Cr-Al and Fe-Cr-Mo have high damping capacities under cyclic loading after being annealed and furnace cooled. This damping capacity is very strain dependent.

5. The somewhat lower level of damping capacity previously reported for a $1000^{\circ}C$ furnace cooled Fe-Cr-Mo alloy was reconfirmed.

B. RECOMMENDATIONS

The following recommendations are proposed for further research and study on high damping Fe-Cr-Al and Fe-Cr-Mo alloys.

1. Further investigation of pseudoelastic effects, through low strain tension-compression testing, should be carried out.

2. Damping measurements should be taken over a wider temperature range, conforming to anticipated operating conditions.

3. The effects of damping at higher strains, higher strain rates, and for longer periods of time, should be studied.

4. Detailed microstructural analysis should be carried out via transmission electron microscopy.

5. The effects on damping capacity of various cooling rates should be studied further.

LIST OF REFERENCES

1. Schetky, L.M. and Perkins, J., "The 'Quiet' Alloys," *Machine Design*, pp. 202-206, 6 April 1978.

2. Reskusich, J., *Cyclic Strain Amplitude and Heat Treatment Effects on the High Damping Behavior of Incramute Alloy Under Random Vibration Loading in the 50-1000 Hz Frequency Range*, M.S. Thesis, Naval Postgraduate School, Monterey, California, September 1986.

3. Naval Underwater Systems Center Report TD 6927, *A Technical Update on Damped Vacrosil-010*, by R.G. Kasper, 19 September 1983.

4. Dew, D.D., *Strain Dependent Damping Characteristics of a High Damping Manganese-Copper Alloy*, M.S. Thesis, Naval Postgraduate School, Monterey, California, September 1986.

5. Leary, L.W., *Damping Behavior of Sonoston and Incramute: Degradation Effects Near Room Temperature*, M.S. Thesis, Naval Postgraduate School, Monterey, California, December 1986.

6. O'Toole, J.F., *Damping Behavior of an Fe-Cr-Mo Alloy: Strain Dependence and Heat Treatment Effects*, M.S. Thesis, Naval Postgraduate School, Monterey, California, December 1986.

7. Cochardt, A.W., "The Origin of Damping in High-Strength Ferromagnetic Alloys," *Transactions of the ASME*, Vol. 75, pp. 196-200, 1953.

8. de Batiste, R., "High Damping Materials: Mechanisms and Applications," *Journal de Physique*, Vol. 44, pp. C9-39-- C9-50, December 1983.

9. Masumoto, H., Sawaya, S., and Hinai, M., "On the Damping Capacity of Fe-Cr Alloys," *Journal of Japan Institute of Metals* (in Japanese), 43, pp. 409-413, 1970.

10. Masumoto, H., Sawaya, S., and Hinai, M., "Damping Characteristics of 'Gentalloy' in the Fe-Mo System," *Transactions of the Japan Institute of Metals*, Vol. 22, No. 9, pp. 607-613, 1981.

11. Masumoto, H., Sawaya, S., and Hinai, M., "Damping Capacity and Pitting Corrosion Resistance of Fe-Mo-Cr Alloys," *Transactions of the Japan Institute of Metals*, Vol. 25, No. 12, pp. 891-899, 1984.

12. Schneider, W., Schrey, P., Hausch, G., and Torok, E., "Damping Capacity of Fe-Cr and Fe-Cr Based High Damping Alloys," *Journal de Physique*, Colloque C5, Supplement au n 10, Tome 42, pp. C5-C35, October 1981.

13. Suzuki, K., Fijita, T., and Haseb, M., "Damping Capacity and Mechanical Properties of Sintered Fe-Cr-Mo High Damping Alloy," *Powder Metallurgy*, No. 4, pp. 205-211, 1977.

14. Willertz, L.E., "Magnetomechanical Damping Properties of AISI 403 Stainless Steel with Applied Static Torsional and Axial Stresses," *Journal of Testing and Evaluation*, JTEVA, Vol. 2, No. 6, pp. 478-482, November 1974.

15. Thomson, W.T., *Theory of Vibrations with Applications*, Prentice-Hall, Inc., 1981.

16. Bert, C.W., "Material Damping: An Introductory Review of Mathematical Models, Measures, and Experimental Techniques," *Journal of Sound and Vibration*, Vol. 29, No. 2, pp. 129-153, 1973.

17. Timoshenko, S., Young, D.H., and Weaver, William, Jr., *Vibration Problems in Engineering*, 4th ed., John Wiley and Sons, Inc., 1974.

18. Reed-Hill, R.E., *Physical Metallurgical Principles*, Brooks/Cole Engineering Div., 1973.

19. Kwabe, H. and Kuwahara, K., "A Consideration of the Strain Amplitude-Dependent Damping and Modulus in Ferromagnetic Metals," *Transactions of the Japan Institute of Metals*, Vol. 22, No. 5, pp. 301-308, 1981.

20. Bolt, Beranek, and Newman, Inc., Cambridge, Massachusetts, "Operations Manual for the Bolt, Beranek, and Newman, Inc., Resonant Dwell Apparatus," January 1973.

21. Peckner, D. and Bernstein, I.M., *Handbook of Stainless Steels*, McGraw-Hill, Inc., 1977.

22. *Metals Handbook*, 8th ed., Vol. 8, American Society for Metals, 1973.

23. The Edward Orton Jr., Ceramic Foundation, Westerville, Ohio, "Operating Instructions--Orton Automatic Recording Dilatometer, Model 15 BC-1."

24. "Standard Methods of Tension Testing of Metallic Materials," ASTM E8-83, American Society for Testing and Materials, Vol. 03.01, pp. 130-150, 1983.

INITIAL DISTRIBUTION LIST

No. Copies

1. Defense Technical Information Center 2
   Cameron Station
   Alexandria, Virginia 22304-6145

2. Library, Code 0142 2
   Naval Postgraduate School
   Monterey, California 93943-5002

3. Professor Jeff Perkins, Code 69 Ps 3
   Department of Mechanical Engineering
   Naval Postgraduate School
   Monterey, California 93943-5004

4. LCDR David B. Ferguson 3
   7298 Oxford Court N. W.
   Bremerton, Washington 98310

5. Mrs. Catherine Wong, Code 2812 3
   David Taylor Naval Ship R & D Center
   Annapolis, Maryland 21402

6. Mr. Robert Hardy, Code 2803 3
   David Taylor Naval Ship R & D Center
   Annapolis, Maryland 21402

7. Dean of Science and Engineering, Code 06 1
   Naval Postgraduate School
   Monterey, California 93943-5000

8. Research Administration, Code 012 1
   Naval Postgraduate School
   Monterey, California 93943-5000

9. Department Chairman, Code 69Hy 1
   Department of Mechanical Engineering
   Naval Postgraduate School
   Monterey, California 93943-5004

10. Professor Y. S. Shin, Code 69Sg 1
    Department of Mechanical Engineering
    Naval Postgraduate School
    Monterey, California 93943-5000

11. Mr. Charles Zanis, Code 196   1
    Naval Sea Systems Command
    Washington, D.C. 20362-5101

12. LCDR Wallace M. Elger, Code 05MB   1
    Naval Sea Systems Command
    Washington, D.C. 20362-5101

13. Mr. A. G. S. Morton, Code 2813   1
    David Taylor Naval Ship R & D Center
    Annapolis, Maryland 21402

14. Mr. V. J. Castelli, Code 2844   1
    David Taylor Naval R & D Center
    Annapolis, Maryland 21402

END

DATE
FILMED
8-88

DTIC